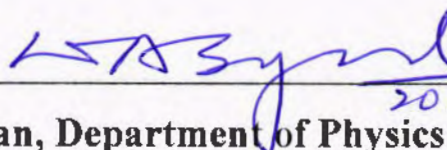# Study of Structural and Dielectric Properties of $(Al_2O_3)_x$/CuTl-1223 Nanoparticles-Superconductor Composite

by:

Khurram Shehzad

(235-FBAS/MSPHY/F13)

Supervisor:

Dr. Muhammad Mumtaz

Assistant Professor
Department of Physics, FBAS,
IIU, Islamabad

Department of Physics

Faculty of Basic and Applied Sciences

International Islamic University, Islamabad

(2016)

Nanoparticles.
Superconducting

Study of Structural and Dielectric Properties of (Al$_2$O$_3$)$_x$/CuTl-1223 Nanoparticles-Superconductor Composite

by:

Khurram Shehzad

(235-FBAS/MSPHY/F13)

This Thesis submitted to Department of Physics International Islamic University, Islamabad for the award of degree of MS Physics.

20.4.16

_____

Chairman, Department of Physics

International Islamic University, Islamabad
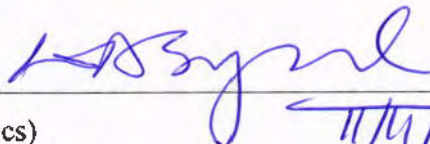
_____

Dean Faculty of Basic and Applied Science

International Islamic University, Islamabad

Final Approval

It is certified that the work printed in this thesis entitled "**Study of Structural and Dielectric Properties of $(Al_2O_3)_x$/CuTl-1223 Nanoparticles-Superconductor Composite**" by **Khurram Shehzad**, registration No.235-FBAS/ MSPHY/ F13 is of sufficient standard in scope and quality for award of degree of MS Physics from Department of Physics, International Islamic University, Islamabad, Pakistan
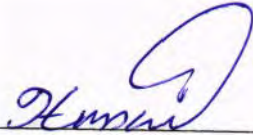
Viva Voce Committee

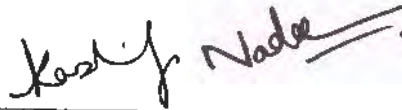Chairman _____

(Department of Physics)

Supervisor _____

External Examiner _____

Internal Examiner _____

بِسْمِ اللَّهِ الرَّحْمَٰنِ الرَّحِيمِ

DEDICATED

to

My beloved

Mother

Grand Father

Father

and

My

Respected teachers

Declaration of Originality

I **Khurram Shehzad** (Registration # 235-FBAS/MSPHY/F13), student of Ms in Physics (session 2013-2015), hereby declare that the matter printed in the thesis titled "**Study of Structural and Dielectric Properties of $(Al_2O_3)_x$/CuTl-1223 Nanoparticles-Superconductor Composite** is my own work and has not been published or submitted as research work or thesis in any form in any other university or institute in Pakistan or aboard.
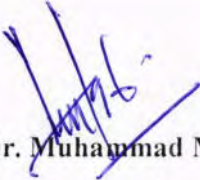
Khurram Shehzad

(235-FBAS/MSPHY/F-13)

Dated; 19 / 04 / 2016

FORWARDING SHEET BY RESEARCH SUPERVISOR

The thesis entitled **"Study of Structural and Dielectric Properties of $(Al_2O_3)_x$/CuTl-1223 Nanoparticles-Superconductor Composite"** submitted by *Khurram Shehzad* in partial fulfillment of M.S. degree in Physics has been completed under my guidance and supervision. I am satisfied with the quality of student's research work and allow him to submit this thesis for further process to graduate with Master of Science degree from Department of Physics, as per IIU rules and regulations.

Dated: 18/04/2016

Dr. Muhammad Mumtaz,
Assistant Professor
Department of Physics,
International Islamic University,
Islamabad.

ACKNOWLEDGMENT

Table of Contents

Figure Contents

Table Contents

Abstract

$(Cu_{0.5}Tl_{0.5})Ba_2Ca_2Cu_3O_{10-\delta}$ superconducting material and alumina (Al_2O_3) nanoparticles were synthesized by solid-state reaction and sol-gel method, respectively. Al_2O_3 nanoparticles were mixed in appropriate ratio to CuTl-1223 matrix to obtain $(Al_2O_3)_x$/CuTl-1223; x = 0, 0.5, 1 and 1.5 wt. % nano-superconductor composites. Structure and phase purity of Al_2O_3 nanoparticles and $(Al_2O_3)_x$/CuTl-1223 nano-superconductor composites were determined by XRD, SEM and EDX techniques. No change in crystal structure of parent CuTl-1223 matrix was observed after addition of Al_2O_3 nanoparticles, which shows that these nanoparticles has occupied the grain-boundaries. The morphology was examined by SEM images, which showed the presence of spherical and irregular shaped Al_2O_3 nanoparticles at the grain-boundaries of CuTl-1223 matrix. The presence of Al_2O_3 nanoparticles has reduced the voids and has improved the inter-grains connectivity. The mass percentage of different elements in the composition was determined by EDX spectroscopy. The dc-resistance verses temperature measurements of these samples were carried out by four-probe technique. Measurements revealed that value of critical temperature "T_c" was suppressed after inclusion of Al_2O_3 nanoparticles into CuTl-1223 matrix. The dielectric properties of these samples (i.e. dielectric constant, dielectric loss and ac-conductivity) were determined by experimentally measured capacitance (C) and conductance (G). Phenomenon of negative capacitance was observed, which may be due to lower Fermi levels of ceramic superconducting sample as compared to contact electrodes The addition of Al_2O_3 nanoparticles in CuTl-1223 matrix has changed the negative values of dielectric parameters irregularly which is associated with non-uniform distribution of these nanoparticles at the inter-granular spaces of CuTl-1223 matrix. The uniform distribution of nanoparticles at the grain-boundaries is the main hurdle. So, we can tune the dielectric properties of CuTl-1223 matrix by uniform distribution of appropriate amount of Al_2O_3 nanoparticles at the grain-boundaries of CuTl-1223.

Chapter 1

Introduction

1.1   Superconductivity

Certain materials have ability to conduct current with zero resistance at certain lower temperature known as critical temperature, such materials are called superconductors and phenomenon is known as superconductivity. Such materials allow current to flow without any energy loss and magnetic field is expelled. Once we setup current in superconductor it can circulate for long time estimated as 10^5 years [1]. Superconductors have variety of applications. Some common examples are high speed magnetic levitation trains, high capacity digital memory chips, radio frequency filters, ultra high speed computers etc. Nanotechnology and superconductivity has transformed scientific world into emerging field of science due to its positive practical and scientific future [2, 3].

1.2   History of superconductors

In 1911, Heike Kamerlingh Onnes, a Dutch physicst, discovered the phenomenon of superconductivity while cooling mercury metal (Hg) to extremely low temperature and observed that the metal exhibited zero resistance to electric current. Fig. 1.1 represent the variation of resistance as a function of temperature for mercury metal.
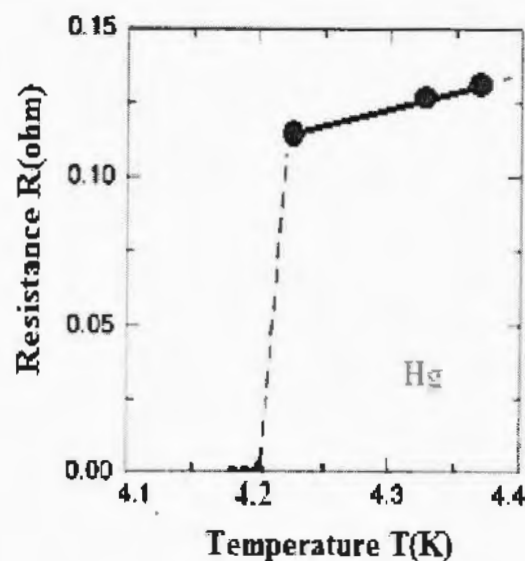
Fig. 1.1: Resistance verses temperature

2

After 1973, many other metals and alloys were found to be superconductors at certain critical temperature T_c. Materials having T_c less than 23.2K are called low temperature superconductors (LTS). Later on in 1986, J. G. Bednorz and K. A. Muller discovered oxide based ceramic materials which demonstrated superconductivity at high temperature ~35K and referred as High Temperature Superconductors (HTS). Fig. 1.2 shows history of discovered superconductors along with their T_C and years of discovery.
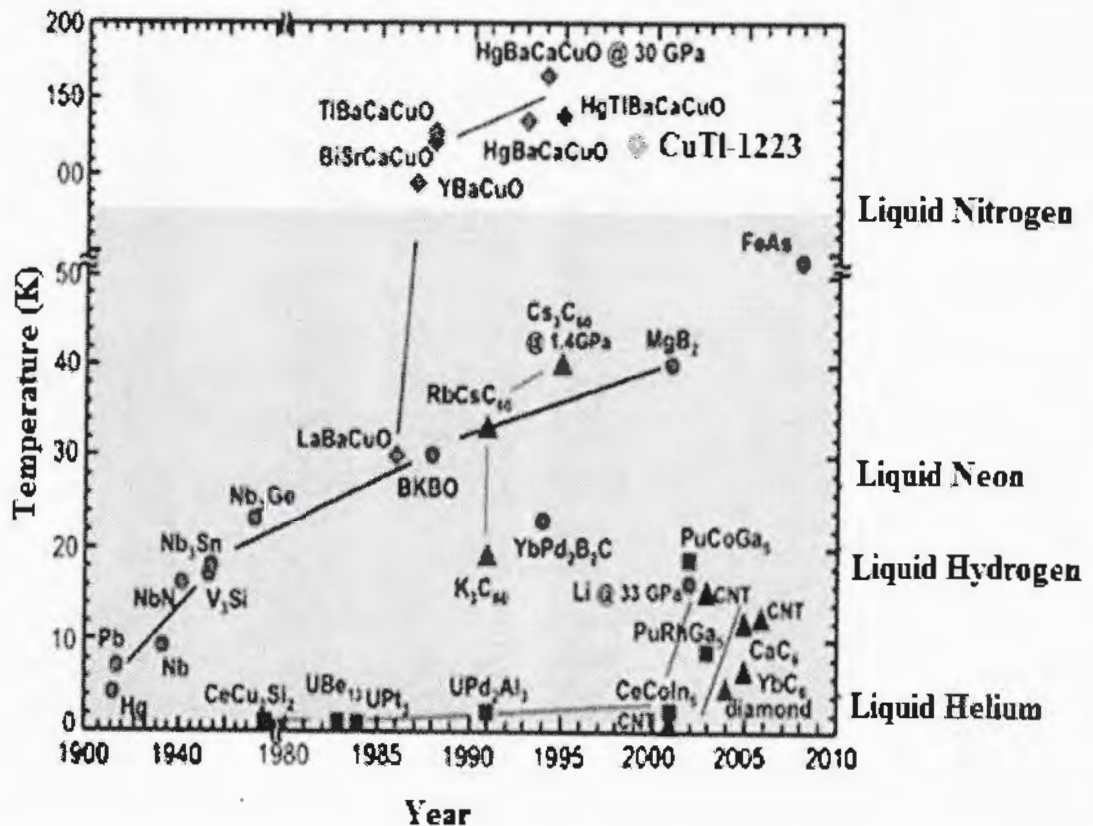
Fig. 1.2: History of discovered superconductors along with their T_C and years of discovery [4].

1.3 Elementary properties of superconductors

1.3.1   Critical temperature (T_c)

Temperature below which material become superconductor is termed as critical temperature [5]. Most of materials have very low critical temperature, such as critical temperature of mercury (Hg) is 4.2K which is difficult to achieve.

Materials having T_c in range of 120K are under high attention due to the reason that they can maintain their superconductivity inside liquid nitrogen having boiling point 77K. Table 1.1 represents different materials with their critical temperatures T_c.

Table. 1.1: Materials and their T_c [6].

Material	Critical temperature
Gallium	1.1K
Aluminium	1.2K
Indium	3.4K
Tin	3.7K
Mercury	4.2K
Lead	7.2K
Niobium	9.3K
La-Ba-Cu-O	17.9K
Y-Ba-Cu-O	92K
Tl-Ba-Cu	125K

1.3.2 Zero electrical resistance

Complete disappearance of electrical resistance is one of most obvious characteristic of superconductors. It happens only below critical temperature. In order to test zero electrical resistance a small electric current is permitted through superconductor. If current does not decay at all, then there exist zero electrical resistance. Electrical resistance of Tl-2223 disappears below128K [7]. Fig. 1.3 represent trend of resistance with respect to temperature.
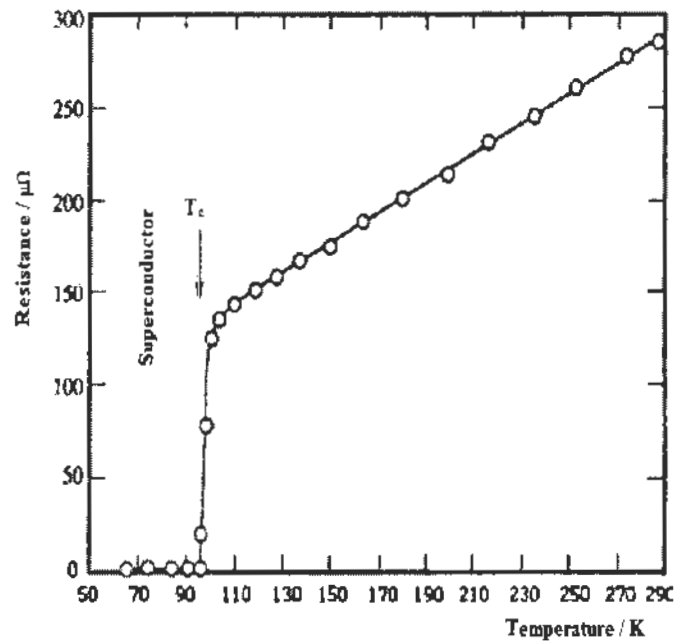
Fig. 1.3: Resistance versus temperature.

1.3.3 Critical current density (J_c)

The value of current density above which a material behave as normal conductor and below which material behave like superconductor is called critical current density J_c [8].

4
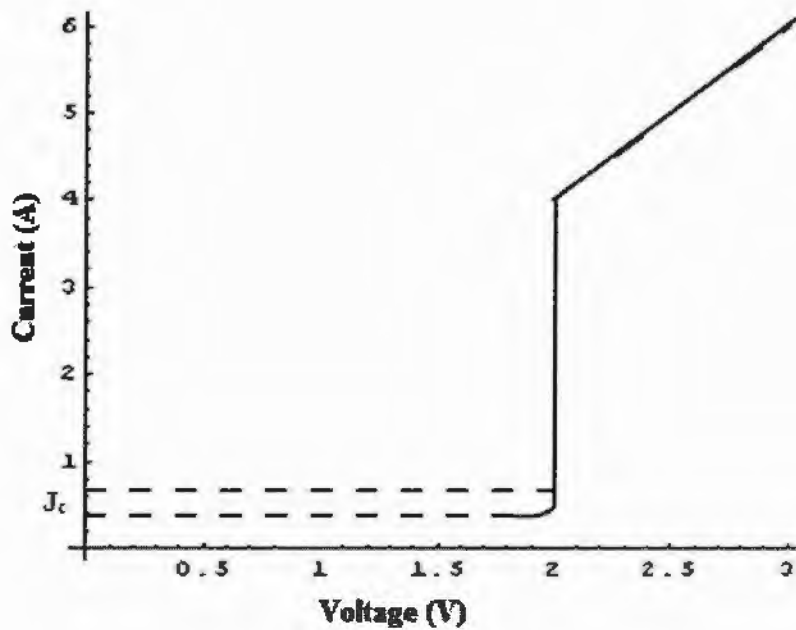
Fig. 1.4: Current verses voltage.

Fig. 1.4 represents that below J_c, voltage remains zero. As the value of current density approaches J_c, material becomes normal conductor and voltage appears across it. For YBCO bulk disk of diameter 0.7cm, material becomes superconductor below 3.08A [9].

1.3.4   Critical magnetic field (B_c)

At particular temperature, maximum value of applied magnetic field where a material can show superconductivity is called critical magnetic field B_c. Above B_c material becomes normal conductor. Shaded region in Fig. 1.5 shows superconducting region.
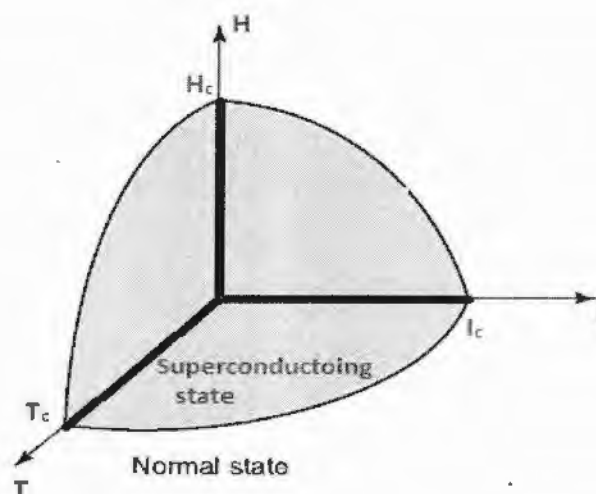
Fig. 1.5: Superconducting state and its critical temperature, field and current density.

It is clear from above discussion that superconductivity strongly depends on critical temperature (T_c), critical magnetic field (B_c) and critical current density (J_c). So all three quantities should be in their critical values for a material to be a superconductor.

1.4   Meissner effect

In 1933, Robert Oschsenfeld and Walter Meissner found a magnetic phenomenon that revealed that superconductors are not only conductors with zero resistivity but also exhibit some other properties [10]. Meissner effect is applicable, when a material becomes superconductor in the presence of magnetic field and an electric current loop appears on its surface. Such currents produces the magnetic field that cancel out externally applied magnetic field, resulting net magnetic field to be zero inside the sample volume, except on surface where currents resides [11,12]. These currents can exist forever without loss of any energy due to zero resistance. Fig. 1.6 shows transition of normal conductor into superconductor
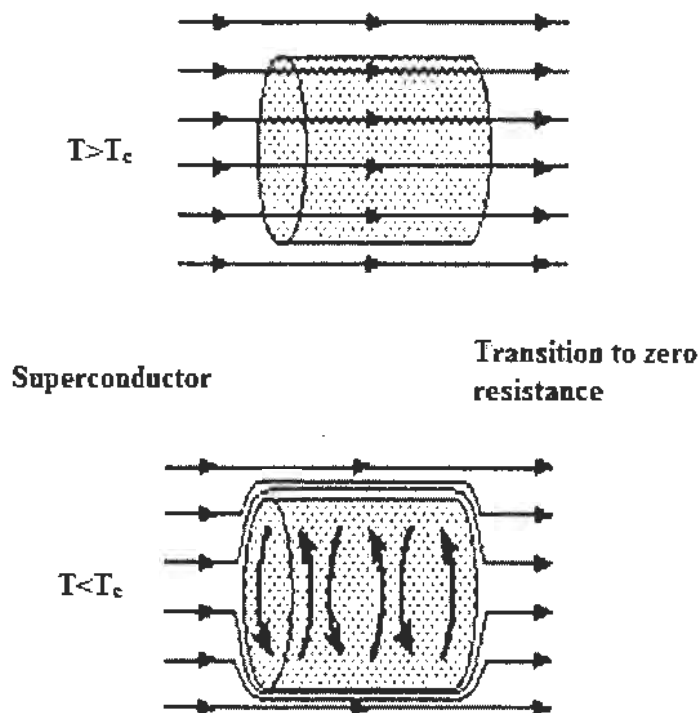
Fig. 1.6: Transition of normal conductor into superconductor.

Meissner effect results from the phenomenon of driven kinetic energy involved in superconductivity. Negative charges are expelled from interior of superconductors to surface generating spin current in superconductors [13].

1.5   Magnetic levitation

If magnetic field applied to sample is caused by magnet, then it will be repelled by magnetic field produced due to inducted currents flowing through superconductor, resulting force to act on magnet. When repulsion force become equal to weight of magnet, then magnet will hang in space over superconductor. Such phenomenon is known as magnetic levitation. Fig. 1.7 represents the schematic view of magnetic levitation.
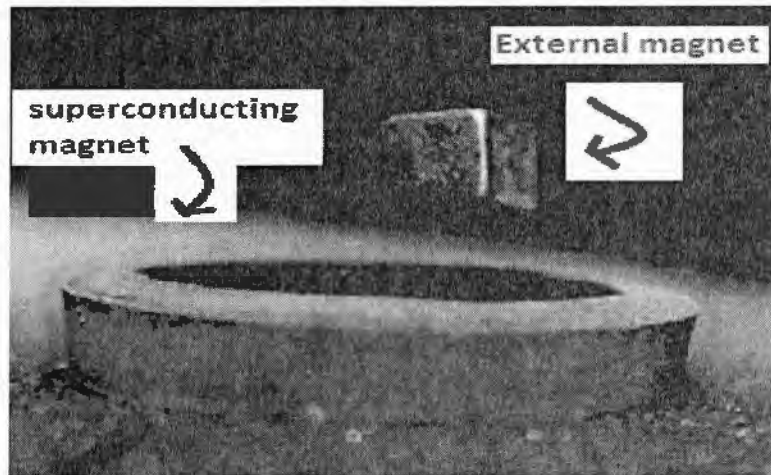
Fig. 1.7: Magnetic levitation.

Superconductive magnetic levitation principle is used in supraTrans transportation. A project designed for passenger transport, maintaining consistency between propulsion safety positioning and systems [14].

1.6   BCS theory

Before 1957, superconductivity was not explained sufficiently. At that time John Bardeen , his assistants Jon Schreiffer and Leon Cooper gave microscopic description of superconductors, known as BCS theory [15]. This earned them Nobel prize later on.

BCS theory is in contradiction to our previous assumptions that is in superconductors electron do not interact with lattice. This theory tells us that electron do interact with atoms constructively. A crucial assumption is taken that there exist an attractive force between electrons which arises due to Coulomb attraction between crystal lattice and electron. An electron increases positive charge around itself in lattice. This positive charge attracts another electron forming Cooper pair as shown in Fig. 1.8. If thermal vibration energy of lattice is less than energy required to bind Cooper pair, then Cooper pair remain bound. This estimates that

why low temperature is required for superconductivity. In superconductors current flows due to Cooper pair rather than single electron.

Resistance of material vanishes because of cooper pairs. An electron causes increase of positive charge around itself inside lattice. As current flows, lagging electron is attracted due to positive charge caused by leading electron.
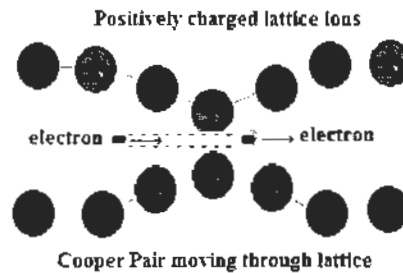
Fig. 1.8: Moving Cooper Pair.

This theory has been verified with help of isotope effect. This shows that critical temperature depends upon mass of nucleus of material atoms. An isotope of greater number of neutron suppresses critical temperature.

BCS theory can be used for investigation of critical temperature, upper critical field and magnetic penetration depth [16].

1.7   Types of superconductors

Superconductors are classified into two categories depending on their physical properties, our interest, how expensive is their cooling, and our understanding about them. Usually superconductors are classified according to their transition from normal to superconducting state. In superconducting state material expels magnetic field and in normal state field passes through material. Thermodynamic stability of vortex effects a lot magnetic response of superconductor. Vortex stability has great impact on ratio of magnetic field during passing through vortex core to critical field. These findings set new criteria for superconductor classification [17].

1.7.1   Type-I superconductor

Type-I superconductors mainly contain metalloids and metals that can show good conductivity even at room temperature. They require very low temperature to show effects

explained by BCS theory i-e electrons pairs up to form Cooper pairs. In this way they overcome resistance of lattice molecules.
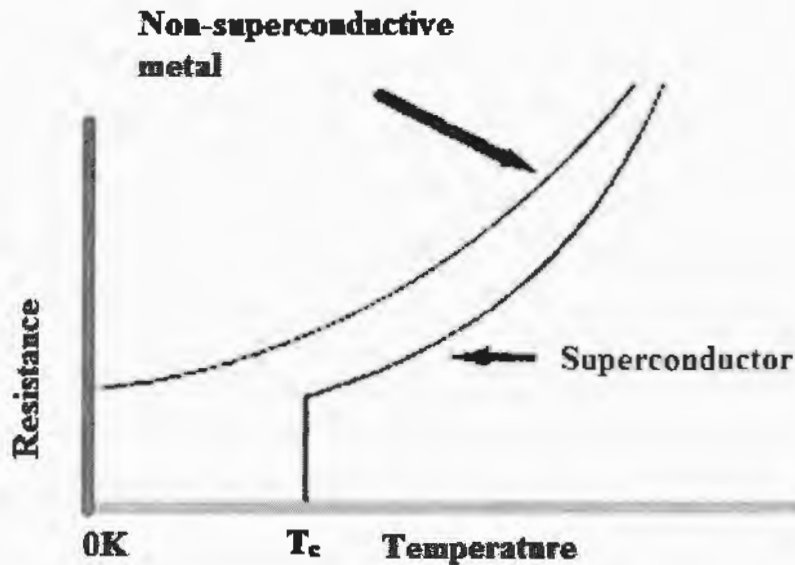
Fig. 1.9: Resistance verses temperature for normal and superconducting state.

Type-I superconductors are also regarded as soft superconductors as they have very low critical temperature. They undergo sharp transition from normal to superconducting state and become diamagnetic as required conditions are imposed. As critical temperature is achieved their resistance suddenly drops to zero as shown in Fig.1.9.
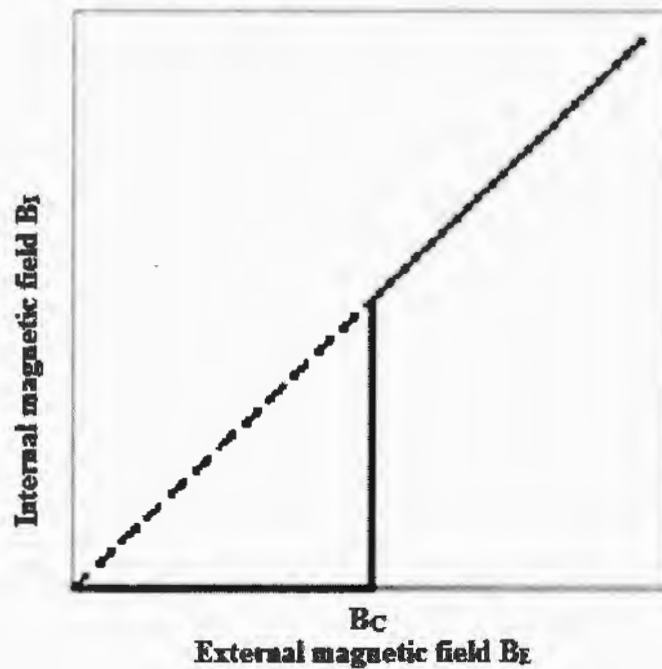
Fig. 1.10: Internal magnetic field and externally applied magnetic field.

Superconductivity can be destroyed due to application of high magnetic field. Fig. 1.10 shows the variations in internal magnetic field with applying external magnetic field. Internal field is zero below critical field. As external field is increased beyond critical field the material becomes normal conductor and field penetrates into material.

Superheated and supercooled field transition of superconductors of Type-I is more demanding in upcoming research. It can be used in superconductive radiation detectors [18].

1.7.2 Type-II superconductors

Such superconductors have critical field ranging from B_{C1} & B_{C2}. If externally applied magnetic field is greater than B_{C2}, than all magnetic field penetrate into material and material behave as normal conductor. For $B_{C1} < B < B_{C2}$, material behave as partially superconductor i-e magnetic field partially penetrate into material as shown in Fig. 1.11 and Fig. 1.12.
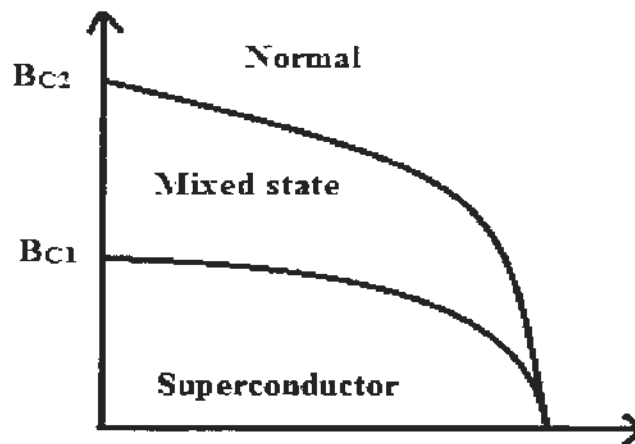
Fig. 1.11: Normal, mixed and superconducting state.

At this stage superconductor material split into two regions: superconductive region from where magnetic field lines are expelled and normal state region where magnetic field lines passes as shown in Fig. 1.13.
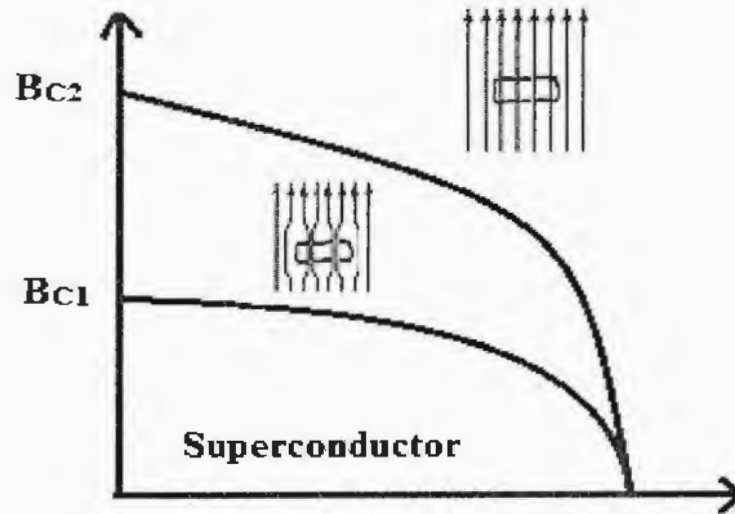
Fig. 1.12: Penetration of magnetic field in normal and superconducting state.

Normal regions behave like filaments filled with external field. At interface between superconductor and normal region electric current flows. This current screens the penetration of magnetic field into superconductive region. Thus current is carried by region of Type II superconductor
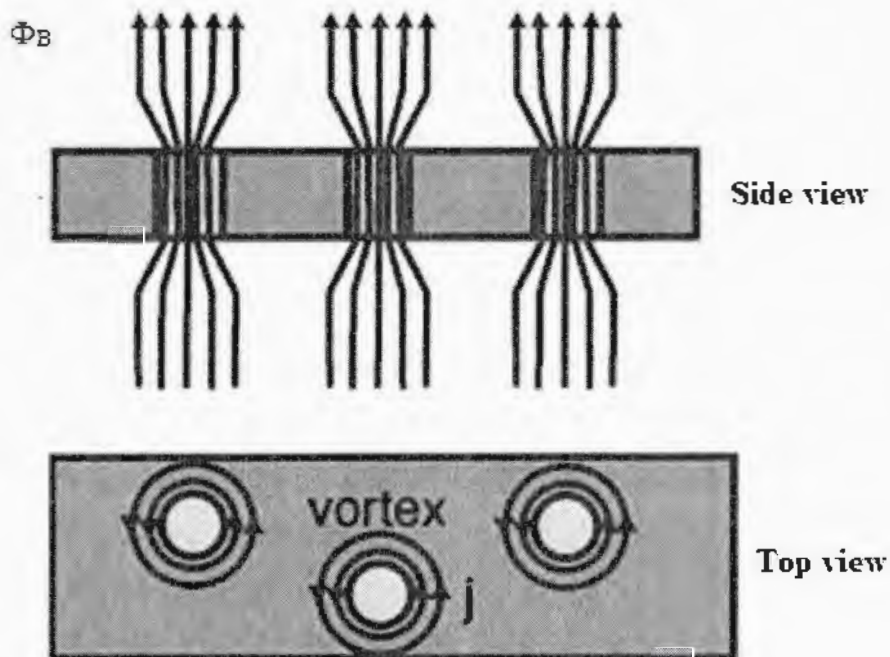
Fig. 1.13: Vortex side view and top view.

As external field B becomes less than B_{C1}, entire material becomes superconductor, magnetic field is entirely expelled through material.

1.8   High temperature superconductors (HTSCs)

Materials like ceramics are expected to have insulating behaviour but surprisingly they do not show behaviour like that.

Table.1.2: Formula, critical temperature, notation, crystal structure and number of Cu-O planes in unit cell of some materials [19].

Formula	T_c (K)	Notation	Crystal structure	No. of Cu-O planes in unit cell
$YBa_2Cu_3O_7$	92	123	Orthorhombic	2
$Bi_2Sr_2CuO_6$	20	Bi-2201	Tetragonal	1
$Bi_2Sr_2CaCu_2O_8$	85	Bi-2212	Tetragonal	2
$Bi_2Sr_2Ca_2Cu_3O_6$	110	Bi-2223	Tetragonal	3
$HgBa_2CuO_4$	94	Hg-1201	Tetragonal	1
$HgBa_2CaCu_2O_6$	128	Hg-1212	Tetragonal	2
$HgBa_2Ca_2Cu_3O_8$	134	Hg-1223	Tetragonal	3
$TlBa_2Ca_3Cu_4O_{11}$	122	Tl-1234	Tetragonal	4
$Tl_2Ba_2CuO_6$	80	Tl-2201	Tetragonal	1
$Tl_2Ba_2CaCu_2O_8$	108	Tl-2212	Tetragonal	2
$Tl_2Ba_2Ca_2Cu_3O_{10}$	125	Tl-2223	Tetragonal	3

. In 1986 Alex Muller and Georg Bednorz investigated the conductivity of lanthanum-barium copper oxide. Critical temperature of 30K was calculated, it was highest T_c up to that time. They found that by adding lanthanum into yttrium, T_C of 92K can be obtained. [20]. This was just beginning of high temperature superconductors. Later on superconductors of higher temperature like $Tl_2Ba_2Ca_2Cu_3O_{10}$ having $T_c = 125K$ was discovered. Table 1.2 shows the crystal structure and corresponding critical temperature of some materials.

1.9   Thallium based superconductors

In family of Tl-Ba-Ca-Cu-O, a number of materials have been studied. All these materials have different charge reservoir layers and number of superconducting planes. Tl-2201 contain double layer of Tl_2O_3 in charge reservoir. Other compounds that belong to family of Tl-Ba-Ca-Cu-O are Tl-2212, Tl-2223 etc. They involve number of CuO_3 planes are represented by last digit. They have values of critical temperature ranging from 80K to 120K. It has been investigated that with increasing number of CuO_3 planes, T_c increases up to 3 planes but decreases for 4 planes due to the presence of intact insulating layers. Such compound is named as $TlBa_2Ca_3Cu_4O_{11}$ having relatively higher resistance at room temperature.

$Cu_{1-x}Tl_xBa_2Ca_3Cu_4O_{12-s}$ superconductors are prepared to overcome problems mentioned above [21,22]. Structure of CuTl-1223 is shown in Fig. 1.14
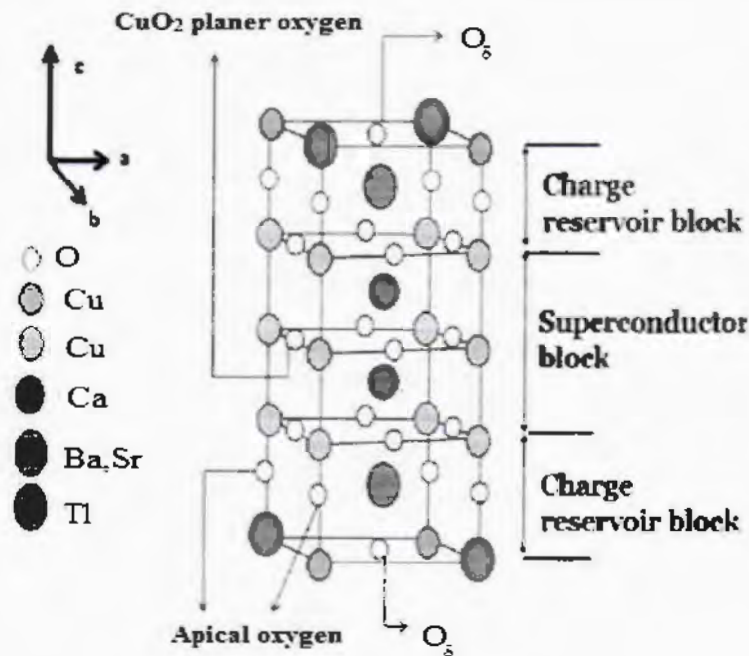
Fig. 1.14: Structure of CuTl-1223.

In 1993 cuprates having T_C 133K were discovered at atmospheric pressure. In 2000 fluorinated materials were found with slight increase in T_C to 138K. This lead to beginning of efforts to find more cuprates with higher T_C [23].

1.10   Coherence length

The interaction of Coulomb repulsion of electron-electron is weaker than lattice-electron interaction at temperature less than critical temperature. At such state, Cooper pairs

do not scatter from lattice i.e. Cooper pairs sail over lattice point smoothly without any dissipation of energy. Hence there is no transfer of energy between crystal lattice and Cooper pair of electron. Whenever an electric field is applied, electron pairs acquire extra kinetic energy and give rise to flow of current. They cannot be slowed down as they are not losing any energy. This shows that material is not possessing any energy at this state. Electrons travel small distances in coupled form of order of 10^{-6}m, known as coherence length. Over this small distance material behave like superconductor [24].

1.11 Penetration depth

London equation explains that magnetic field decays exponentially inside the superconductor with increasing distance. In superconductors, the thickness of material through which current flows is 10^{-5}cm [25]. For stronger superconductors this thickness decreases. When an external magnetic field is applied, current must flow through this layer to cancel magnetic field. Magnetic field decays exponentially as we move from surface to inside of superconductor. If B(0) is magnetic field at surface, then magnetic field at any depth x can be found as,

$$B(x) = B(0) \exp(-x/\lambda_L) \qquad (1.1)$$

Where λ_L is knows as penetration depth. Fig. 1.15 shows relation between magnetic field and depth [26-28]
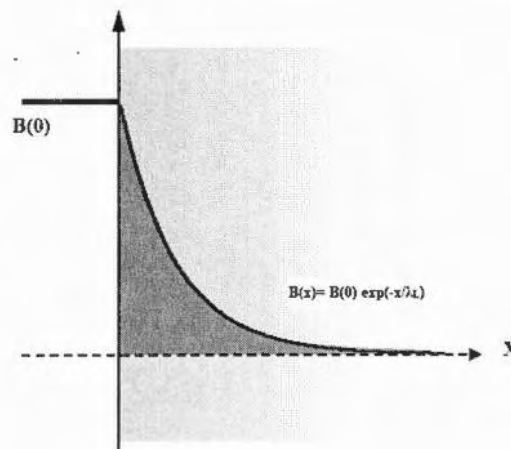
Fig. 1.15: Depth and applied field.

1.12   Dielectric

Materials having insulating properties and high dielectric constant are referred as dielectric materials. When a dielectric is placed between plates of a capacitor, its capacitance increases by factor k_e given as:

$$C = C_o \, k_e \qquad (1.2)$$

Where k_e is called dielectric constant, C_o and C are capacitances before and after placing dielectric material respectively. For all dielectric materials value of k_e is always greater than 1.

There are two types of dielectrics, polar dielectrics and non-polar dielectrics.

1.12.1 Polar dielectric

Electric dipole moment stays permanent in case of polar dielectrics. One of vital example of polar dielectric is water.
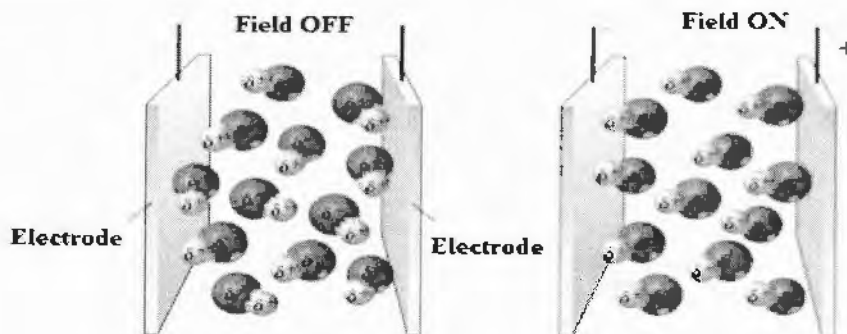
Fig. 1.16: Dipole moments in absence and presence of field.

In absence of externally applied electric field, polar molecules exist in random orientations. While in the presence of external electric field, torque act on dipoles and align the dipoles such that positive ions faces negative electrode and negative ions faces positive electrode as shown in Fig. 1.16. These aligned dipoles generate an electric field having magnitude smaller then externally applied electric field but in opposite direction.

1.12.2 Non-polar dielectric

Dipole moments in non-polar dielectrics are not permanent. Electric dipole moments appear when an external electric field is applied. Fig1.17 represents the phenomenon of electric dipole formation in non-polar dielectric materials.
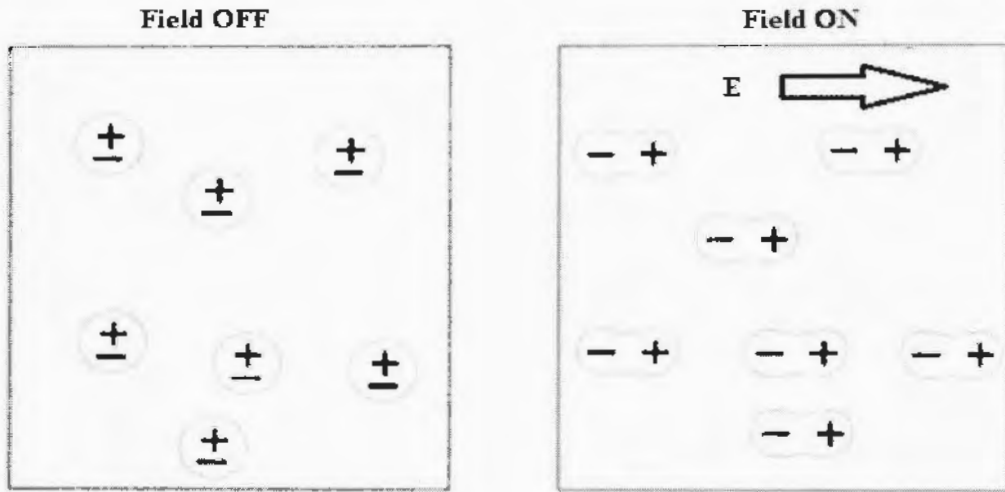
Fig. 1.17: Alignment of dipoles in absence and presence of electric field.

Electric field is induced due to polarization of molecules in opposite direction to applied field [29]. The resultant field can be calculated as

$$E = E_o + E_p \qquad (1.3)$$

Where E_p is polarized field, E_o is applied field and E is resultant field. Net field is weaker as compared to applied field because polarized field is in opposite direction to applied field, so minimize its effect. Electric field after placing dielectric can be calculated by following equation

$$E = E_o / k_e \qquad (1.4)$$

Where k_e is referred as dielectric constant.

1.13 Polarization

Separation of charges when the dielectric material is subjected to external electric field is known as polarization. In the absence of external electric field each electric dipole presents its own electric field.

Generally polar molecules are randomly oriented. When they are placed inside electric field produced by the charged capacitor, then dipole moments are oriented in one particular direction so that their electric fields cancel external field. Presence of such dielectric material reduces electric potential across plates of capacitor as shown in Fig. 1.18.

16

Vacuum   **Dielectric**

Voltmeter   **Voltmeter**
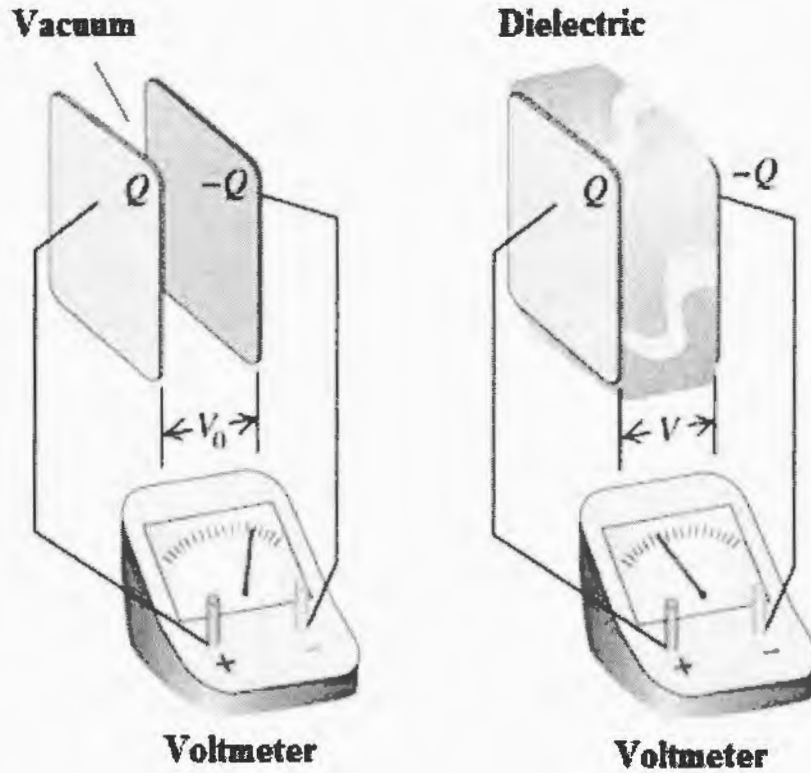
Fig. 1.18: Electric potential between plates with vacuum and dielectric material.

Reduction of potential difference results an increase in capacitance of capacitor by a factor k_e, called dielectric constant.

Vacuum having permittivity ε_o

Capacitance = C

(a)   (b)
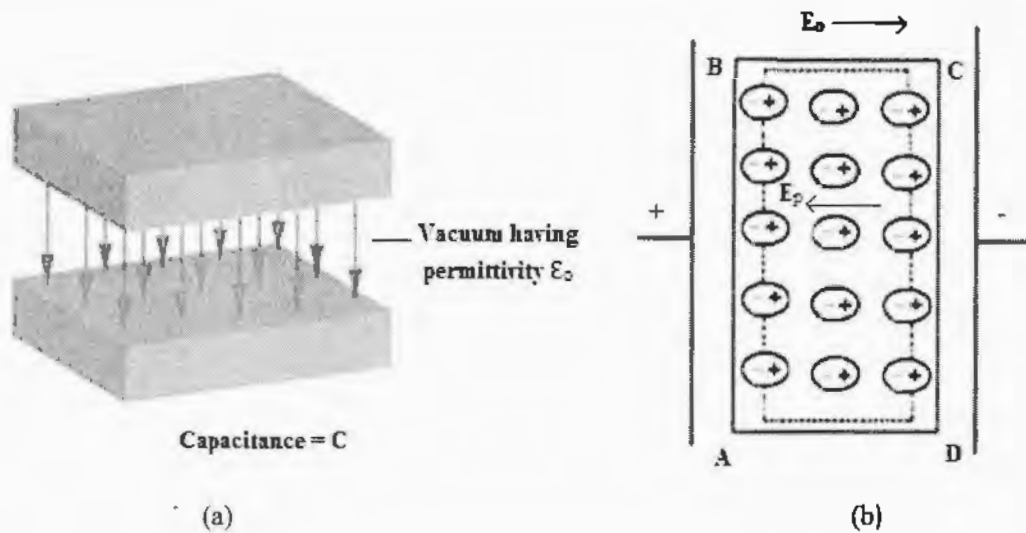
Fig. 1.19: a) Capacitor without dielectric b) capacitor with dielectric.

Fig. 1.19 a) shows capacitor in absence of dielectric medium and its capacitance can be found by using equation given below

$$C = A\mathcal{E}_o/d \qquad (1.5)$$

Fig. 1.20 b) shows dielectric material that is placed between plates of capacitor, it enhances capacitance by factor as shown in equation given below

$$C_m = A\mathcal{E}_o k_e/d \qquad (1.6)$$

Where A is area of one plate facing other, $\mathcal{E}_o$ is permittivity of free space, d is spacing between plates and k_e is called dielectric constant. Hence polarization enhances the charge storing capacity of capacitor.

1.13.1 Types of polarization

Net polarization consists of four sub types of polarizations

1.13.1.1 Ionic polarization

In dielectrics there exist ionic bonding. Anions and cations are displaced in opposite directions due to application of external electric field. Ionic polarization occurs due to shifting of ions with respect to their neighbouring opposite charges.

No Applied Field
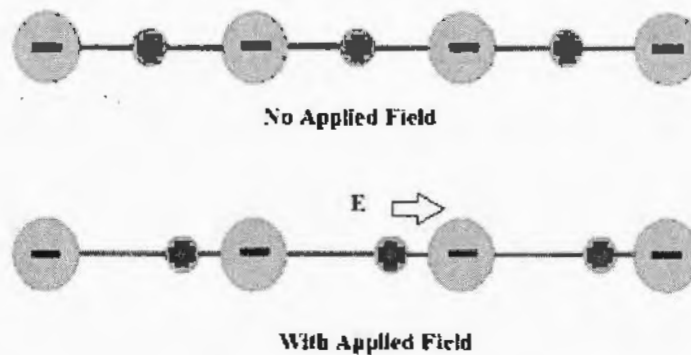
With Applied Field

Fig. 1.20: Shifting of ions due to application of external electric field.

Fig 1.20 shows that positive ions shift in the direction of applied field and negative ions shift opposite to direction of applied field. Ionic polarization is independent of temperature. So occurs at all temperatures.

1.13.1.2 Orientation or dipolar polarization

In dielectric materials natural dipoles rotate freely, (e-g in gaseous or liquid materials) are called polar dielectrics. In such materials molecular dipoles are liable to orient along direction of applied electric field. Such alignment of molecules results in polarization of materials.
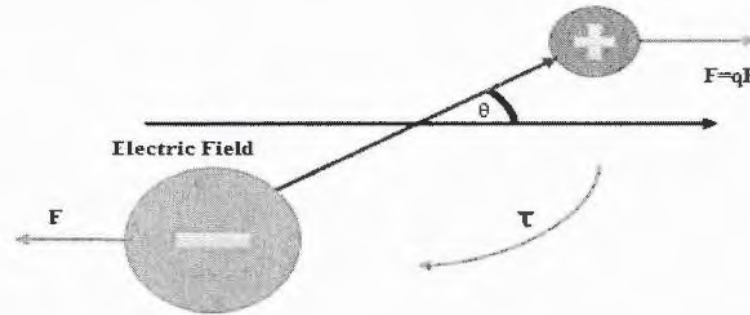
Fig. 1.21: Couple acting on dipole due to external field.

Fig.1.21 shows that dipole tend to orient in direction of electric field up to an angle θ. Dipolar polarization is also independent of temperature.

1.13.1.3 Space charge polarization

In such polarization, charge accumulation increases at electrodes or in multiphase materials at interfaces. When external electric field is applied, ions diffuse over reasonable distance and results into new distribution of charges.

Fig.1.22 shows redistribution of charges due to application of external electric field. Space polarization is strongly temperature dependent [30].
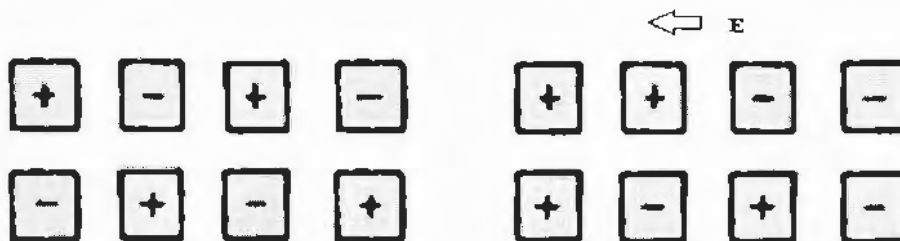
Fig. 1.22: Rearrangement of charges due to external field.

1.13.1.4 Electronic polarization

Electronic polarization takes place due to retaliation of individual atoms on application of external electric field. It is also known as atomic polarization. In this process electrons of an atom displace in direction opposite to that of applied field while nucleus displace in direction of applied field. Such phenomenon is known as dipole movement inside an atom.

Fig 1.23 shows shifting of nucleus and electrons on application of external electric field. Electronic polarization doesn't depend on temperature and is directly proportional to strength of applied electric field.

Fig. 1.23: Shifting of electrons opposite to applied field.

1.14 Frequency dependence of dielectric

Orientation of dipole moments and shifting of ions and charges changes periodically along the direction of externally applied field, as ac field is applied. Usually high frequency field is applied to dielectric. When high energy electromagnetic radiations are incident on dielectric, it is clear from electromagnetic theory that refractive index affects dielectric constant in range of optical frequency. Such affect is shown by equation given below;

$$K_e = n^2 \qquad (1.7)$$

Electronic polarization lasts up to high frequency UV range as it is a fast process, ionic polarization can exist up to frequency of infrared range as it is slower process. Dipolar polarization can only exist up to frequency of microwave range, as it is slowest process.

1.15 Nanotechnology

Technology which deals with exploitation of very small systems of order of 10^{-9}m is called nanotechnology. One nanometre is millionth part of a millimetre. One of example of such system is human hair which is about 50,000 nanometres in diameter. In this system, materials have amazingly different properties e.g. difference in colour, conductivity, reactivity etc. Nanomaterial has much improved properties as compared to bulk, therefore nanotechnology so far has great impact on all types of technologies e-g Medical, agriculture, engineering, industries etc.

Caroline E. Handford *et al.* investigated that current time awareness of nanotechnology is low in agri-food, neither positive nor negative response is shown by respondents. Priority of people was found to be safer food, increased product and reduced waste. Practical use of agri-food applications is not up to mark. They interviewed 14 agri-food stakeholders and gathered response of 88 agri-food stakeholders via online website [31].

1.17   Nanomaterials and their classification

In European commission, a material is said to be nanomaterial if it one or more dimensions exist in range of 1nm-100nm.According to ISO, nanomaterials are the materials that have internal or external dimension in nanoscale.

Nano-materials are categorized into four types, depending upon their dimensions in nanoscale.

Table.1.3: Types of materials and their examples.

Material type	Example
Zero-dimensional nanomaterial: Materials having all dimensions less than 100nm.	 Clusters (0D)
One-dimensional nanomaterial: Materials baving two dimensions less than 100nm and one dimension in bulk	 Nanotubes, fibres and rods (1D)
Two-dimensional nanomaterial: Materials having one side at nanoscale and two sides in bulk	 Coats and films (2D)
Three dimensional nanomaterial: Materials having all sides in bulk, such materials are nanobased materials	 Polycrystals (3D)

1.18   Synthesis of nanoparticles

Nano-particles can be synthesised by using two basic techniques given below

I)   Bottom up technique

II)   Top down technique

In bottom up technique, molecules, atoms, ions are placed together to construct a particle known as nano-particle. It is further explained in Fig. 1.24.

Bottom Up

Fig. 1.24: Bottom up technique.

In top down technique etching, ball milling and attrition methods are used for synthesis of nanoparticles. In this approach structure defects are very crucial, any defect can change properties of nano-particles significantly. This technique is explained in Fig 1.25 given below.

Top Down

Fig. 1.25: Top down technique.

Nanoparticles can also be synthesized chemically. In this technique we use sol-gel, hydrothermal, colloidal emulsion and co-precipitation method. By using this technique we can efficiently control chemical composition and morphology of compound. Sol-gel and co-precipitation methods are commonly used for synthesis of nanoparticles.

Fig. 1.23: Shifting of electrons opposite to applied field.

1.14 Frequency dependence of dielectric

Orientation of dipole moments and shifting of ions and charges changes periodically along the direction of externally applied field, as ac field is applied. Usually high frequency field is applied to dielectric. When high energy electromagnetic radiations are incident on dielectric, it is clear from electromagnetic theory that refractive index affects dielectric constant in range of optical frequency. Such affect is shown by equation given below;

$$K_e = n^2 \qquad (1.7)$$

Electronic polarization lasts up to high frequency UV range as it is a fast process, ionic polarization can exist up to frequency of infrared range as it is slower process. Dipolar polarization can only exist up to frequency of microwave range, as it is slowest process.

1.15 Nanotechnology

Technology which deals with exploitation of very small systems of order of 10^{-9}m is called nanotechnology. One nanometre is millionth part of a millimetre. One of example of such system is human hair which is about 50,000 nanometres in diameter. In this system, materials have amazingly different properties e.g. difference in colour, conductivity, reactivity etc. Nanomaterial has much improved properties as compared to bulk, therefore nanotechnology so far has great impact on all types of technologies e-g Medical, agriculture, engineering, industries etc.

Caroline E. Handford *et al.* investigated that current time awareness of nanotechnology is low in agri-food, neither positive nor negative response is shown by respondents. Priority of people was found to be safer food, increased product and reduced waste. Practical use of agri-food applications is not up to mark. They interviewed 14 agri-food stakeholders and gathered response of 88 agri-food stakeholders via online website [31].

1.15.1 Nanoscience

Science that deals with study of manipulation of matter at molecular, atomic and macromolecular scale is called nano-science. Polymers are prepared by using nano scale subunits. Nano based materials have much larger surface to size ratio, therefore such materials are more reactive, their chemical properties and electrical properties have improved dramatically. In nanoscience quantum effects dominate, resulting change in electrical, optical and magnetic behaviour [32].

1.16 History of nanotechnology

Nanotechnology is an old concept come from Greek word dwarf while its emerging is relatively new in scientific research. Due to small size, it is hard to study nano based materials. Developments made in this field, after invention of advance experimental techniques like scanning tunnelling microscope in 1981 and invention of fullerenes in 1985.There are few names, which played important role in emerging nanotechnology.

Richard Feynman thought that there exist a field in which not so much has been done. This field cannot be understood by fundamental physics, but solid state physics give some clue about it. At small scale things can be controlled. There exists some strange phenomenon in complex situations. Large number of technical applications can be accessed by using this technique [33].In Dec 29, 1959 annual meeting of American Physical Society, Dr. Feynman gave transcript "There is plenty of Room at bottom"

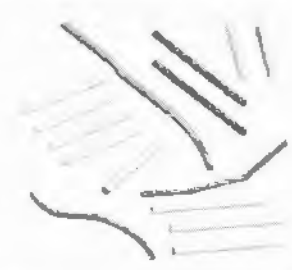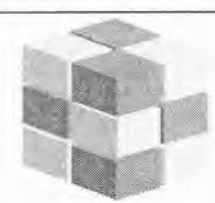In 1974 professor Norio Taniguchi used the term nanotechnology very first time at Tokyo Science University. It was used to express extension of traditional silicon machining into smaller than one micron regions. Now a days it is commonly used in engineering with objects smaller than 100nm
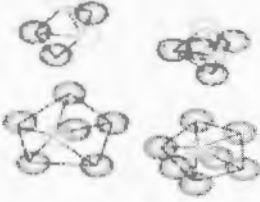
K. Drexler is considered as Godfather of nanotechnology. He provided a minuscule robot sea that could position molecules quickly and precisely so that any substance can be produced by using ordinary ingredients. In blood flow small machines can be flown and used to cure diseases. K. Eric Drexler got attentions of younger people, they buy the idea which are neat things and can be done by thinking small.

1.17 Nanomaterials and their classification

In European commission, a material is said to be nanomaterial if it one or more dimensions exist in range of 1nm-100nm.According to ISO, nanomaterials are the materials that have internal or external dimension in nanoscale.

Nano-materials are categorized into four types, depending upon their dimensions in nanoscale.

Table.1.3: Types of materials and their examples.

Material type	**Example**
Zero-dimensional nanomaterial: Materials having all dimensions less than 100nm.	 Clusters (0D)
One-dimensional nanomaterial: Materials having two dimensions less than 100nm and one dimension in bulk	 Nanotubes, fibres and rods (1D)
Two-dimensional nanomaterial: Materials having one side at nanoscale and two sides in bulk	 Coats and films (2D)
Three dimensional nanomaterial: Materials having all sides in bulk, such materials are nanobased materials	 Polycrystals (3D)

1.18   Synthesis of nanoparticles

Nano-particles can be synthesised by using two basic techniques given below

I)   Bottom up technique

II)   Top down technique

In bottom up technique, molecules, atoms, ions are placed together to construct a particle known as nano-particle. It is further explained in Fig. 1.24.
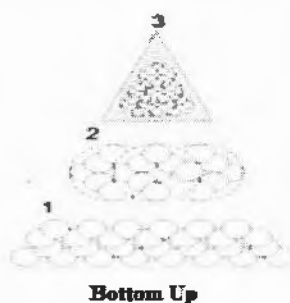
Fig. 1.24: Bottom up technique.

In top down technique etching, ball milling and attrition methods are used for synthesis of nanoparticles. In this approach structure defects are very crucial, any defect can change properties of nano-particles significantly. This technique is explained in Fig 1.25 given below.
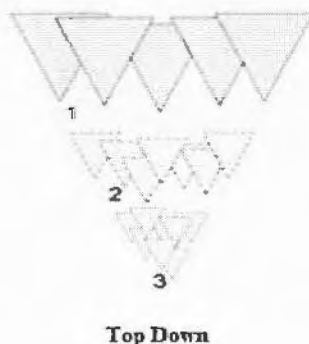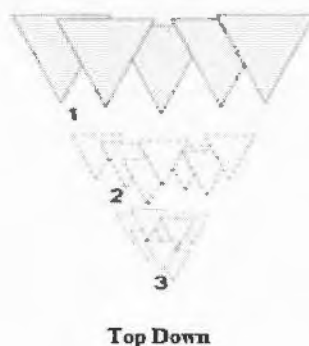
Fig. 1.25: Top down technique.

Nanoparticles can also be synthesized chemically. In this technique we use sol-gel, hydrothermal, colloidal emulsion and co-precipitation method. By using this technique we can efficiently control chemical composition and morphology of compound. Sol-gel and co-precipitation methods are commonly used for synthesis of nanoparticles.
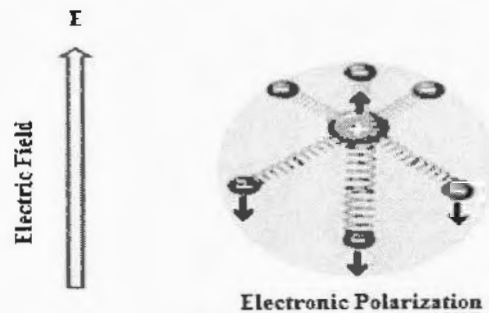
1.18.1 Sol-gel method

In this process monomers are converted into colloidal solution (sol). Such solutions act as precursor for integration of particles or polymers. Solution is evolved towards gel like system containing both solid phase and liquid phase. Stages involved in sol-gel method are shown in Fig. 1.26. Sol-gel method was used for characterization of hybrid scaffolds and hierarchical structure of silicate glass that are used for regeneration of bone [34].
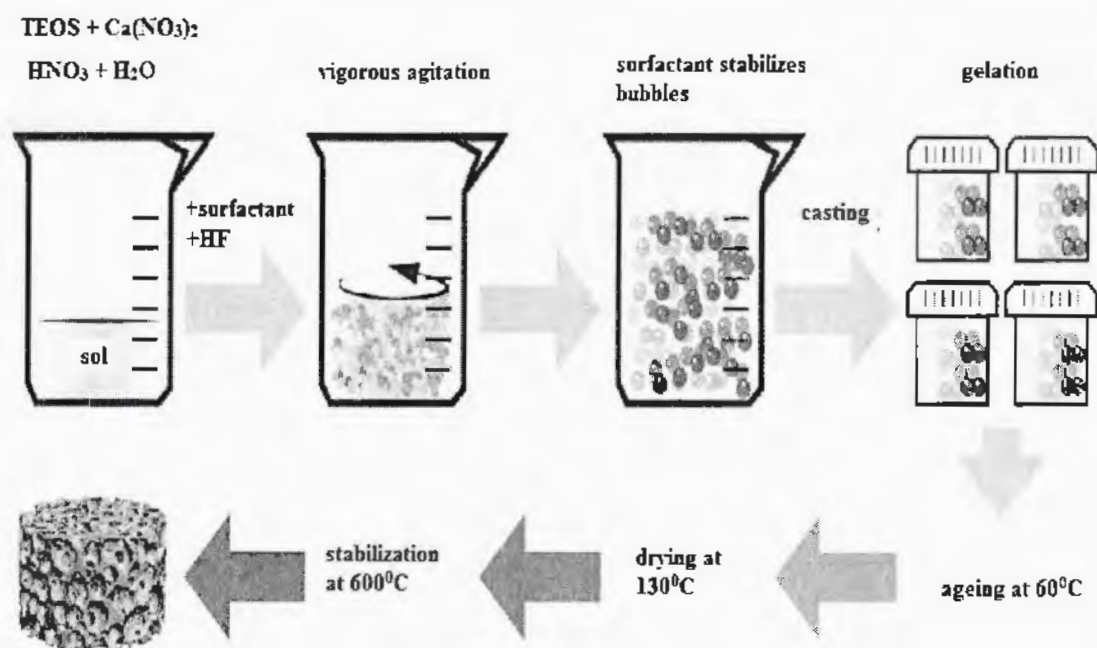
Fig. 1.26: Stages involved in sol-gel method.

Low pressure and low temperature based nanoparticles can be synthesised by sol-gel method. Moreover nanoparticles prepared by such technique have high purity level and tapered size distribution [35].

1.18.2 Co-precipitation method

It is a chemical method which involves nucleation, coarsening, growth and agglomeration process [36]. The obtained nanoparticle has narrow particle size and uniform distribution. During this process precipitate can be collected in the form of oxalates, carbonates or hydroxides[37].

Steps involved in co-precipitation method are shown in Fig 1.27.
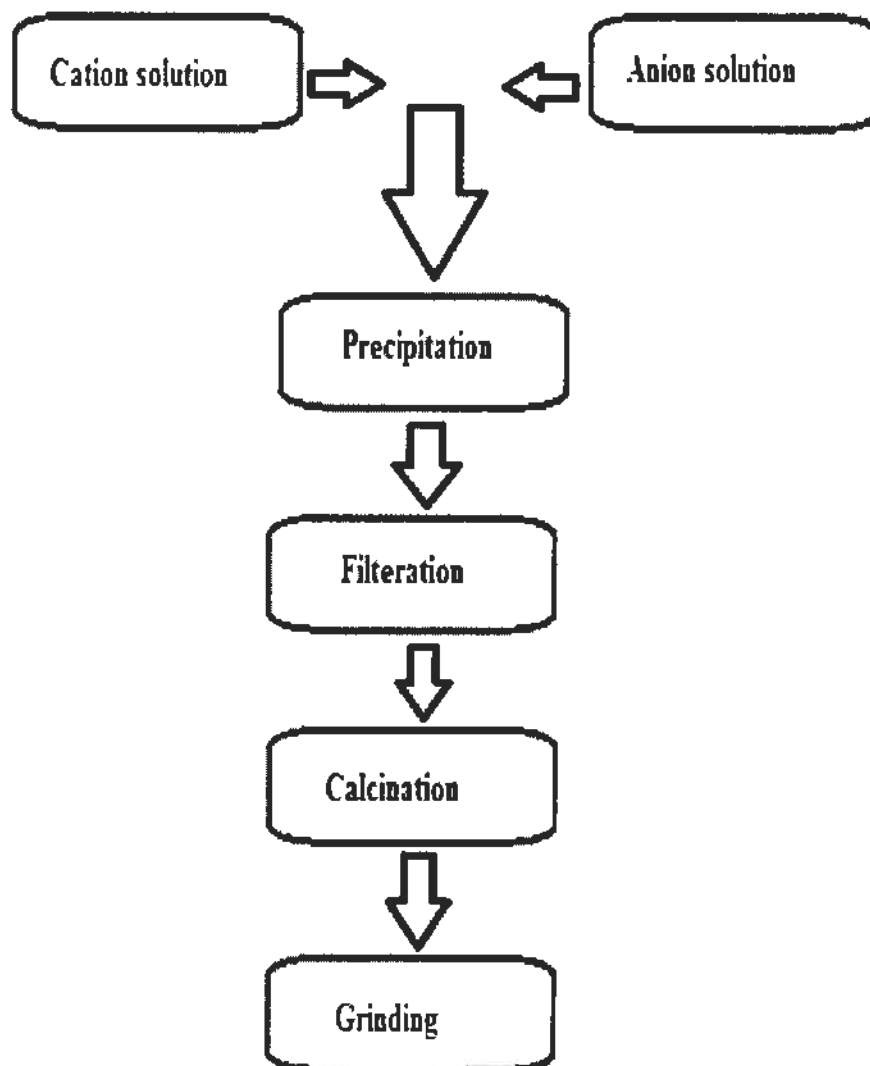
Fig. 1.27: Stages involved in Co-precipitation method.

References

1. M. Tinkham, "Introduction to superconductivity" second Edition, P.213 (2004).

2. J.J Powell, N. Faria, E. T. Mickay and L.C. Pele, "Origin and fate of dietary nanoparticles and microparticles in the gastrointestinal tract" J. Auto. Chem. **34**, 226 (2010).

3. S. K. Sahoo, S. Parveen and J. J. Panda, "The present and future of nanotechnology in human health care" Nanomedicine **1**, 20 (2007).

4. www.kjmagnetics.com.

5. L. Cooper "Bound electron pairs in a degenerate Fermi gas" Phys. Rev. B **104**, 1189 (1956).

6. www.hyperphysics.phy.astr.gsu.edu.

7. R. S. Liu, J. L. Tallon and P.P. Edwards, "An efficient and reproducible approach for attaining superconductivity at 128 K in $Tl_2Ba_2Ca_2Cu_3O_{10-\delta}$" Physica C **182**, 119 (1991).

8. D. Dimos, P. Chaudhari and J. Mannhart, "Superconducting transport properties of grain boundaries in $YBa_2Cu_3O_7$ bicrystals" Phys. Rev. B **41**, 4038 (1990).

9. N. Hosseini, S. Kananian, A. Zabetian and M. Fardmanesh, "Point Contact Based Method to Measure Critical Current Density of Superconductor Bulk" Phy. Procedia. **36**, 655 (2012).

10. D. D. Hughes. "Flux pinning mechanisms in type II superconductors" Philos. Mag. **30**, 2 (1974).

11. A. M. Campbell, and J. E. Evetts, "Flux vortices and transport currents in type II supercondutros" Adv. Chem. Phys. **50**, 1249 (2001).

12. A. M. Campbell, J. E. Evets and D.D. Hughes, "Pinning of Flux Voritces in Type II superconductor" Phil. Mag. B **18**, 313 (1968).

13. A. Changjan and P. Udomsamuthirun, "The critical magnetic field of anisotropic two-band magnetic supercondutors" Solid State Commun. **151**, 988 (2011).

14. S. Rosenzweig, E. Reich, V. Neu, D. Berger, K. Peukert and B. Holzapfel, "A Superconducting levitation transport model system for dynamical and didactical Studies" Supercond. Sci. Technol. **36**, 242 (2012).

15. D. Pines, "Superconductivity in the Periodic System" Phys. Rev. **109**, 280 (1958).

16. W. Pindt and E. Schachinger, "Is a BCS-like theory sufficient to describe the superconducting state of Y-Ba-Cu-O?" Phys. B. **165**, 1091 (1990).

17. J. P. Wang, "Stability of vortex in a two-component superconductor" Phys. Rev. B **82**, 132 (2010).

18. J. Seco and T. A Girard, "The supercritical fields of metastable Type I superconductors" Nucl. Instrum. Methods Phys. Res., Sect. A **444**, 357 (2000).

19. http://2012books.lardbuckct.org/books/principles-of-general-chemistry-v1.0/s12-09-polar-covalent-bonds.html.

20. A. Schilling, M. Cantoni, J. D. Guo and H. R. Ott, "Superconductivity above 130 K in the Hg–Ba–Ca–Cu–O system" Nature **56**, 363 (1993).

21. H. Ihara, "How to achieve the best performance superconductor based on Cu-1234" Physica C **364**, 289 (2001).

22. A. Crisan, A. Sarkar, P. Mikheenko, V. S. Kang, M. M. A. Kechik and J. S. Abell, "Improvement of pinning force and critical current density in thick $YBa_2Cu_3O_{7-\delta}$ films grown on $SrTiO_3$ substrates decorated with $LaNiO_3$ nanodots" J. Sup. Novel Magn. **22**, 631 (2009).

23. S. N. Putilin, E.V. Antipov, A. M. Abakumov, M. G. Rozova, K. A Lokshin, D. A. Pavlov, A. M. Blagurov, D. V. Sheptykov and M. Marezio, "Effect of fluorination and high pressure on the structure and properties of the Hg-bearing superconducting Cu-mixed oxides" Physica C **52**, 338 (2000).

24. A. A. Abrikosov, " Magnetic properties of superconductors of the second group" Soviet Phys. JETP **5**, 1174 (1957).

25. A. C. Rose Innes and E. H. Rhoderick, "Introduction to superconductivity" 2nd edition, Pergamon Press Oxford Uk, P.70 (1969).

26. A. Pourret, H. Aubin, J. Lesueur, C. A. Marrache-Kikuchi, L. Bergé, L. Dumoulin and K. Behnia, "Observation of the Nernst signal generated by fluctuating cooper pairs" Nature Physics **2**, 683 (2006).

27. V. Raghavan, "Material science and engineering", fourth edition, eastern company edition, P.686 (1998).

28. A. Pimenov, A. Loidl, B. Schey, B. Stritzker, G. Jakob, H. Adrian, A. V. Pronin and Yu. G. Goncharov, "Universal relationship between the penetration depth and the normal-state conductivity in YBaCuO" Europhys. Lett. **48** 73 (1999).

29. J. R. Christman, "fundamental of solid state" P.421 (1988).

30. Steve, W. Martin, W. Yao and K. Berg, "Space charge polarization measurements as a method to determine the temperature dependence of the number density of mobile cations in ion conducting glasses" Z. Phys. Chem. **223**, 1379 (2009).

31. C. E. Handfor, M. Dean, M. Spence, M. Henchion, C. T. Elliott and K. Campbell, "Awareness and attitudes towards the emerging use of nanotechnology in agri-food sector" Food Control **57**, 24 (2015).

32. Nanoscience and nanotechnology by R. Soc. P.30 (2004).

33. Fenman, " There is plenty of food ta bottom" Eng. and sci. **23**, 322 (1960).

34. R. A. Martin, S. Yue, J. V. Hanna, P. D. Lee, R. J. Newport, M. E. Smith and J. R. Jones, "Characterizing the hierarchical structures of bioactive sol–gel silicate glass and hybrid scaffolds for bone regeneration" R. Soc. **10**, 23 (2012).

35. H. J. Hah, "Preparation of silver nanoparticles through alcohol reduction with organoalkoxysilanes" J. Sol-Gel Sci. Technol. **26**, 467 (2003).

36. J. Sjoblom, R. Lindberg and S. E. Friberg, "Microemulsions-phase equilibria characterization, structures, applications and chemical reactions" Adv. Colloid Interface Sci. **65**, 125 (2005).

37. T. Omata, Y. Goto and S. O.Y. Matsuo, "Nanocystals of zirconia and ceria-based solid electrolytes synthesis and properties" Sci. Technol. Adv. Mater. **8**, 524 (2007).

Chapter 2

Literature Review

Electrical instruments of all types use dielectric materials in any form, connecting wires or cables are insulated by materials called dielectrics. Dielectric materials may be composed of solids, liquid and gas materials. It can be a piece of plastic, mineral oil or nitrogen gas. In industrial coatings parylene is used as dielectric barrier to protect substrate from environment. In electrical transformer mineral oil is used as fluid dielectric. Free space or air is also used as dielectric in parallel plate capacitors. Piezoelectric materials, amplifiers, rectifiers comprises of insulating materials (dielectrics). Now a days there is great scope of using superconductor nanoparticles added as dielectric materials. Bi-Sr-Ca-Cu-O is doped with nanoparticle Pb to form a superconductor with high T_c phase transition Maeda *et al.* [1]. Solid dielectric materials are used in commercially prepared capacitors. Materials which show high permittivity are known as capacitor dielectrics. Such materials can be used to store greater charge at given voltage

$$\sigma_\varepsilon = \varepsilon \frac{V}{d}$$

Capacitance is

$$C = A \frac{\sigma_s}{V} = \frac{A\varepsilon}{d}$$

Above equations shows that charge storage depends upon permittivity of medium [2].

Tin doped cobalt ferrite nanoparticles were prepared by using chemical co-precipitation method of diameters 20 ± 2nm. Dielectric and conductivity behaviour of nanoparticles was enhanced in cobalt ferrite nanoparticles. At low frequency, dielectric behaviour was observed due to grain boundaries. High value of dielectric constant was observed due to shell present around nanoparticles and grain boundaries. Conduction is affected by both grains and grains boundaries [3].

Sanjesh Babu *et al.* prepared $CaCu_3Ti_4O_{12}$ by using modified solid state reaction method. They observed dielectric properties, measured dielectric constant and dielectric loss whilst varying temperature from 303K to 573K and frequency ranges from 102 Hz upto 106 Hz. It was observed that both dielectric constant and tangent loss were dependent on frequency

and temperature. Tangent loss and dielectric constant were increased with decrease in frequency, it is possibly due to interfacial polarization. The applied electric field blocked charge carriers inside grains [4].

Dielectric measurements and infrared absorption spectra of bismuth pyrostannate $Bi_2(Sn_{0.95}Cr_{0.05})_2O_7$ were studied with temperature 110-525K and frequency ranging from 350-1100/cm. Split absorption lines for four frequency regions were distinguished. Maximum behaviour of permittivity was measured in frequency range of 1-200kHz at temperature 100-400K [5].

Z. Lijuan *et al.* studied the dielectric properties and relative defect for concentration of $BaTi_{1-x}Sn_xO_3$ as function of doping concentration of Sn. Dielectric properties were found to be dependent on Sn content. Dielectric properties decreases with increase in doping concentration of Sn. Dielectric properties also depended on relative defect concentration, at higher defect concentration permittivity decreases [6].

A. Younis *et al.* inquired the effect of doping in $Cu_{0.5}Tl_{0.5}Ba_2Ca_3Cu_{4-y}Zn_yO_{12-\delta}$ where y varies from 0-3. Samples having dimensions 2mm x 2.5mm x 10mm were used for characterization techniques. Dielectric properties, ac-conductivity and conductance were investigated in superconducting states and normal states. Negative capacitance observed was due to difference in Fermi energy level of ceramics and electrodes. Charge carriers flows from ceramics towards electrodes due to higher Fermi level of ceramics. Comparison between $Tl_2Ba_2Ca_2Cu_2O_x$ and $Cu_{0.5}Tl_{0.5}Ba_2Ca_3Cu_{4-y}Zn_yO_{12-\delta}$ displayed higher ac conductivities and lower losses. This difference was due to variation in thickness of layers of charge reservoir and polarization that is associated with separation of charges between CuO_2/ZnO_2 planes and $Cu_{0.5}Tl_{0.5}Ba_2O_{4-\delta}$ [7].

M. Mumtaz *et al.* conducted an enquiry into dielectric properties of $Cu_{0.5}Tl_{0.5}Ba_2Ca_2(Cu_{3-y}M_y)O_{10-\delta}$ with frequency variation ranging from 10Khz to 10MHz. Samples with dimensions 2mm x 2.5mm x 10mm were used and observed the phenomenon of negative capacitance. At low frequency and temperature large values of negative dielectric constant were examined, this was due to enhancement of polarizability because of reduction in thermal vibrations of atoms. Dielectric loss was reduced due to polarization that arised from charge carriers between the planes of CuO_2/MO_2 and charge reservoir layers of $Cu_{0.5}Tl_{0.5}Ba_2O_{4-\delta}$. Mobile charge carriers from the planes of CuO_2/MO_2 were displaced from their mean position when external ac-field was applied [8].

Frequency dependent and temperature dependent dielectric properties of CuTl-1234 were inspected by M. Mumtaz *et al.* Frequency ranges from 10KHz to 10 MHz and temperature varies from 78K to 290K. Higher values of dielectric constant were monitored for Tl-based superconductors as compared to CuTl-1234 materials [9].

Frequency dependent dielectric properties of samples $(CuO, CaO_2$ and $BaO)_y$ / CuTl-1223 were examined at different frequencies ranging from 10KHz to 10MHz and temperature varies from 78K-300K. Dielectric constant was decreased while ac-conductivity was enhanced with increase in frequency [10,11].

$Ca_{0.67}La_{0.22}Ti_{(1-x)}Cr_xO_3$ with x = 0 and x = 0.1 $(CLT_{(1-x)}Cr_x)$ samples were prepared by high temperature solid state reaction method. Structural and dielectric properties of sample were studied by X-ray diffraction and dielectric characterizations. Material showed ferroelectric behaviour for x=0 and relaxor behaviour for x=0.1. High permittivity was observed for $CLT_{0.9}Cr_{0.1}$ which open the way of its use in capacitor applications. Dielectric loss was observed that may be due to changing in oxygen vacancy concentrations [12].

Dielectric and structural properties of Fe after inclusion into ZnO. Prepared sample is $Zn_{1-x}Fe_xO$ where x varies from 0-0.03 and synthesised by solution combustion method. Polarization disappeared after increasing frequency beyond a certain limit. Real part, imaginary part and tangent loss was inhibited with increasing concentration of Fe [13,14].

Dielectric properties of $CaLaAlO_4$ ceramic samples were investigated with frequency ranging from $20-10^7Hz$ at temperature varying from 25-700°C. giant dielectric behaviour of sample was observed above 100 °C. This behaviour was reported as two thermally activated dielectric relaxations. Low temperature relaxation was caused due to bulk response of oxygen vacancies hopping motion and high temperature relaxation was due to grain boundaries [15].

Microwave dielectric properties and sinterability of Li_2SnO_3 co-doped with MgO-LiF were studied. Sample was prepared by conventional solid-state route. Addition of LiF lowered sintering temperatures to 880°C and promoted $Li_2Mg_3SnO_6$ formation. Microwave dielectric properties optimized for Li_2SnO_{3-8} wt% MgO with increasing contents of $Li_2Mg_3SnO_6$. Excellent dielectric properties were found at 880oC for for Li_2SnO_3-8 wt% MgO-2 wt% LiF ceramics. Such materials were found to be well suitable for applications in low-temperature co-fired ceramics and compatible with Ag electrodes [16].

The oxygen contents in $Cu_{0.5}T_{l0.5}Ba_2Ca_3(Cu_{4-y}Cd_y)O_{12-x}$ superconductor oxygen post annealing was carried out. Sample was prepared by solid state reaction method. Sample was bar shaped of size 2mm x 2.5mm x 10mm. Dielectric properties and ac-conductivity are probed. Phenomenon of negative capacitance was uttered. Dielectric properties were inhibited except tangent loss, which was increased due to oxygen post annealing. Dielectric properties were varying due to oxygen intake by the sample. At normal state polarizability was lower and thermal agitation was higher due to which dielectric loss is increased and dielectric constant was decreased. Dielectric behaviour strongly depended on temperature and frequency [17].

Satreerat K. Hodak *et al.* fabricated coplanar capacitors and their dielectric behaviour is investigated in frequency range of 1 MHz to 2 GHz and temperature ranges from 300K to 4K. They used off-axis pulsed laser deposition technique to prepare Epitaxial strontium titanate ($SrTiO_3$) thin films on neodymium gallate ($NdGaO_3$) substrate at 820 ^{0}C temperature. Ti/Au coplanar capacitors electrodes with 25 μm gap separation, gap width of 1.5 mm and overall size used was 3mm, synthesised by photolithography and evaporation method. Dielectric properties were enhanced by lowering surface to volume ratio and increasing in-plane grain size [18].

Dielectric properties of $Ba_xSr_{1-x}TiO_3$ were calculated with variation of external electric field by using near-surface inhomogeneous distribution of polarization and thermodynamic model. It was found that dielectric properties of sample strongly depend on externally applied electric field. These results were shown great improvement in understanding of dielectric behaviour of supperlattice with externally applied electric field [19].

K. Yoshii *et al.* looked into dielectric properties of Bi_2CuO_{4x} at frequency ranging from 1kHz to 1MHz. There was monotonic decrease in dielectric constant with increasing frequency of applied field such behaviour was referred as dielectric dispersion. This was because of lacking of spatial coherence of dielectric response. Tangent loss express for activation energy, it suggested that electron hoping between Cu ions were responsible for the dielectric response [20].

Dielectric properties and DC electrical conductivity for carbon nano tubes (CNTs) were observed after mixing of potassium bromide (0-5 wt%) by using percolation theory. CNTs were fabricate by vapour deposition method. DC conductivity of samples supressed with increasing CNTs in compound. Dielectric function was observed at room temperature with different frequencies ranging from 10Hz to 200kHz. Real and imaginary parts of sample for

different CNTs percentages were studied as function of frequency. Sample showed maximum dielectric constant for 1.5wt% of CNTs [21].

M. M Hoque *et al.* examined the dielectric properties of $Sr_3(MgTa_2)O_9$ and $Sr_3(ZnTa_2)O_9$. Samples were prepared by using solid state ceramic method. SMT Pallets of 1.61 mm and 10.05 mm thickness and diameter were used respectively whereas for SZT pallet, thickness and diameter were 1.56 mm and 9.91 mm respectively. Variation of imaginary part, real part with frequency was examined. At low frequency a plateau was monitored for ε'' that fell suddenly with increasing frequency. At certain frequency a broad peak was observed in ε''. Width of relaxation peak was too large in ε'' and it drops with growing temperature. This imitate that sample is not following mono-dispersive curve [22].

G. Kumar *et al.* fabricated $Mg_{0.9}Mn_{0.1}Co_xFe_{2-x}O_4$ by solution combustion technique. Dielectric behaviour of Mg-Mn nanoferrites were caught out at room temperature. Size of particle used was 20.9 nm to 23.9 nm. Dielectric constant decreased with increasing concentration of cobalt ions. Dielectric loss and dielectric constant decreased with increasing frequency [23].

S. S. Jadhav *et al.* inspected dielectric properties of $Ni_{1-x}Zn_xFe_2O_4$ ferrites with variation of frequency and temperature. Sample was synthesised by co-precipitation technique. Phenomenon of dispersion in dielectric constant was traced with frequency. Dielectric loss decreased with increasing frequency. Dielectric constant was increased with increasing temperature and composition, and decreased with increasing frequency [24].

S. M. Khetre *et al.* synthesised $LaFeO_3$ by using combustion method having size of 28-63 nm. Dielectric dispersion is observed with frequency, this is due to electron-hole hoping process which caused polarization and conduction. Such materials are useful for fabrication of gas sensors, solar cell etc [25].

References

1. H. Maeda, Y. Tanaka, M. Fukutumi, and T. Asano, "A new high-Tc oxide superconductor without a rare earth element " Jpn. J. Appl. Phys. **27**, 209 (1988).

2. Mussig & H. Joachim, "Semiconductor capacitor with praseodymium oxide as dielectric" U.S. Patent **113**, 388 (2004)

3. A. Rahman, M. A Rafiq, M. Hasan, M. Khan, S. Karim and S. Oh. Cho "Enhancement of electrical conductivity and dielectric constant in Sn-doped nanocrystlline $CoFe_2O_4$" Springer, **15**, 121 (2013).

4. S. Babu and A. Govindan, "Dielectric properties of $CaCu_3Ti_4O_{12}$ (CCTO) prepared by modified solid state reaction method" Int. Rev. Appl. Eng. Res. **4**, 275 (2014).

5. S. S. Aplesnin, L. V. Udod, M. N. Sitnikov and N. P. Shestakov, "$Bi_2(Sn_{0.95}Cr_{0.05})_2O_7$: Structure, IR spectra, and dielectric properties" Ceram. int. **42**, 5177 (2015).

6. Z. Lijuan, W. Lihai, L. Jiandang, C. Bin, Z. Minglei and Y. Bangjiao, "Dielectric properties and structural defects in $BaTi_{1-x}Sn_xO_3$ ceramics" J. Phys. **443**, 166 (2014).

7. A. Younis and N. A. Khan, "Dielectric properties of $Cu_{0.5}Tl_{0.5}Ba_2Ca_3Cu_{4-y}Zn_yO_{12-\delta}$ (y = 0, 3) Superconductors" J. Korean Phys. Soc. **57**, 1437 (2010).

8. M. Mumtaz, N. A. Khan and S. Khan, "Frequency dependent dielectric properties of $Cu_{0.5}Tl_{0.5}Ba_2Ca_2(Cu_{3y}M_y)O_{10-\delta}$ superconductor" J. Appl. Phys. **111**, 216 (2012).

9. M. Mumtaz, Nawazish and A. Khan, "Dielectric properties of $Cu_{0.5}Tl_{0.5}Ba_2Ca_3Cu_4O_{12-\delta}$ bulk superconductor" Physica **469**, 728 (2009).

10. M.Mumtaz, M Kamran, K. Nadeem, M. A Jabbar, A Saleem and S. Hussain, "Dielectric properties of $(CuO,CaO_2,$ and $(BaO)_y$/CuTl-1223composites" J. Low Temp. Phys. **39**, 806 (2013).

11. S. Sarkar, N. S. Das and K. K. Chattopadhyay, "Optical constants, dispersion energy parameters and dielectric properties of ultra-smooth nanocrystalline $BiVO_4$ thin films prepared by RF magnetron sputtering" Solid state sci. **33**, 58 (2014).

12. A. B. Hassen, F. I. H. Rhouma, J. Dhahri and N. Abdelmoula, "Effect of the substitution of titanium by chrome on the structural, dielectric and optical properties in $Ca_{0.67}La_{0.22}Ti_{(1-x)}Cr_xO_3$ perovskites" J. Alloys Compd, **663**, 436 (2016).

13. M. L. Dinehsa, G. D. Prasanna, C. S. Naveen and H. S. Jayanna. "Structural and dielectric properties of Fe doped ZnO nanoparticles " J. Indian Phys. **87**, 147 (2012).

14. M. Hassan, A. S. Ahmed, M. Chaman, W. Khan, A. H. Naqvi and A. Azam, "Structural and frequency dependent dielectric properties of Fe^{3+} doped ZnO nanoparticles" Mater. Res. Bull. **47,** 3952 (2012).

15. J. Zhang, Y. Li, D. Zhang, H. C. Qi, X. X. Xu, Z.F. Huang and C. C. Wang, "Giant dielectric behaviour in $CaLaAlO_4$ ceramics" Mater. Lett. **168,** 163 (2015).

16. Z. Fu, P. Liu, J. Ma, B. Guo, X. Chen and H. Zhang, "Microwave dielectric properties of low-fired Li_2SnO_3 ceramics co-doped with MgO–LiF" Mater. Res. Bull. **77,** 78 (2016).

17. M. Mumtaz, M. Rahim, Nawazish A. Khan, K. Nadeem and K. Shehzad, "Dielectric properties of oxygen post-annealed $Cu_{0.5}Tl_{0.5}Ba_2Ca_3(Cu_{4-y}Cd_y)O_{12-\delta}$ bulk superconductor" Ceram. Int. **39,** 9591 (2013).

18. S. K. Hodak and C. T. Rogers, " Microstructure and dielectric response of $SrTiO_3/NdGaO_3$ interdigitated capacitors" Microelectron. Eng. **85,** 444 (2008).

19. D. Li and F. Ling, "dielectric properties of $Ba_xSr_{1-x}TiO_3$ thin films on a compliant substrate" Int. J. for Light and Electron Opt. **127,** 3766 (2016).

20. K. Yoshii, T. Fukuda, H. Akahama, J. Kano, T. Kambe and N. Ikeda, "Magnetic and dielectric study of Bi_2CuO_4" Physica C **471,** 766 (2011).

21. S. Dadras and M. V. Farahani, "The effects of carbon nano tubes on electric and dielectric properties of CNTs doped KBr (CNTs/KBr) compound" Physica B, **477,** 94 (2015).

22. M. M. Hoque, A. Dutta, S. Kumar and T. P. Sinha, "Sturctural and dielectric properties of $Sr_3(MgTa_2)O_9$ and $Sr_3(ZnTa_2)O_9$" Physica B. **468-469,** 85 (2015)

23. G. Kumar, R. Rani, S. Sharma, K. M. Batoo and M. Singh, "Electric and dielectric study of cobalt substituted Mg-Mn nanoferrites synthesized by solution combustion technique" Ceram int. **39,** 4813 (2013).

24. S. S. Jadhav, S. E. Shirsatha, B. G. Tokshab, D. R. Shengulea and K. M. Jadhavb, "Structural and dielectric properties of Ni-Zn ferrite nanoparticles prepared by co-precipitation method" Comm. & Sci. **431,** 509 (2008).

25. S. M. Khetrea, H. V. Jadhav, P. N. Jagadale, S. R. Kulal and S. R. Bamane, "Studies on electrical and dielectric properties of $LaFeO_3$" Adv. Appl. Sci. Res. **4,** 503 (2011)

Chapter 3

Synthesis Techniques and Characterizations

3.1   High temperature superconductor synthesis

So for number of methods have been used for preparation of pure phase of high temperature superconductors [1,2]. Most effective method I have found is solid state reaction method. It has been used widely for formation of high temperature superconductors based on oxide. In this method various compounds are heated to high temperature after mixing thoroughly.

3.2 Sample preparation

3.2.1   Synthesis of alumina by sol-gel method

Chemicals used for synthesis of Al_2O_3 were NaOH and $Al(NO_3)_3.9H_2O$. Aqueous solution of 2M HNO_3 and $Al(NO_3)_3.9H_2O$ were mixed with a stirrer for 5min. Now 1M NaOH is added into solution drop wise at room temperature and stirred continuously. PH of solution noted finally after 2 hours when precipitation takes place. These precipitates were bathed and accumulated with the help of distilled water. Then precipitates were left for drying process at 100^0C for overnight. Powder obtained was calcinated for 5 hours at 200^0C in oven. That's how alumina was obtained.

3.2.2   CuTl-1223 superconductor synthesis

For synthesis of CuTl-1223 ($Cu_{1-x}Tl_xBa_2Ca_2Cu_3O_{10-s}$) superconductor matrix I used solid state method. Three compounds $Cu_2(CN)_2.H_2O$, $Ba(NO_3)_2$ and $Ca(NO_3)_2$ with appropriate ratio were mixed and grounded with mortar and pestle for 2 hours. Then I placed that mixture in furnace for 24 hours at 860^0C. Furnace was switched off after 24 hours of heating process, I waited for furnace temperature to come at room temperature. After that I took sample out of furnace and again grounded it with mortar and pestle for 2 hours. Then again placed sample in pre-heated chamber furnace for 24 hours sintering at 860^0C. Again it was switched off and precursor was ready as it came to room temperature. Now I added an appropriate mass of thallium oxide 1.7gm in precursor. This can also be explained in Fig. 3.1.
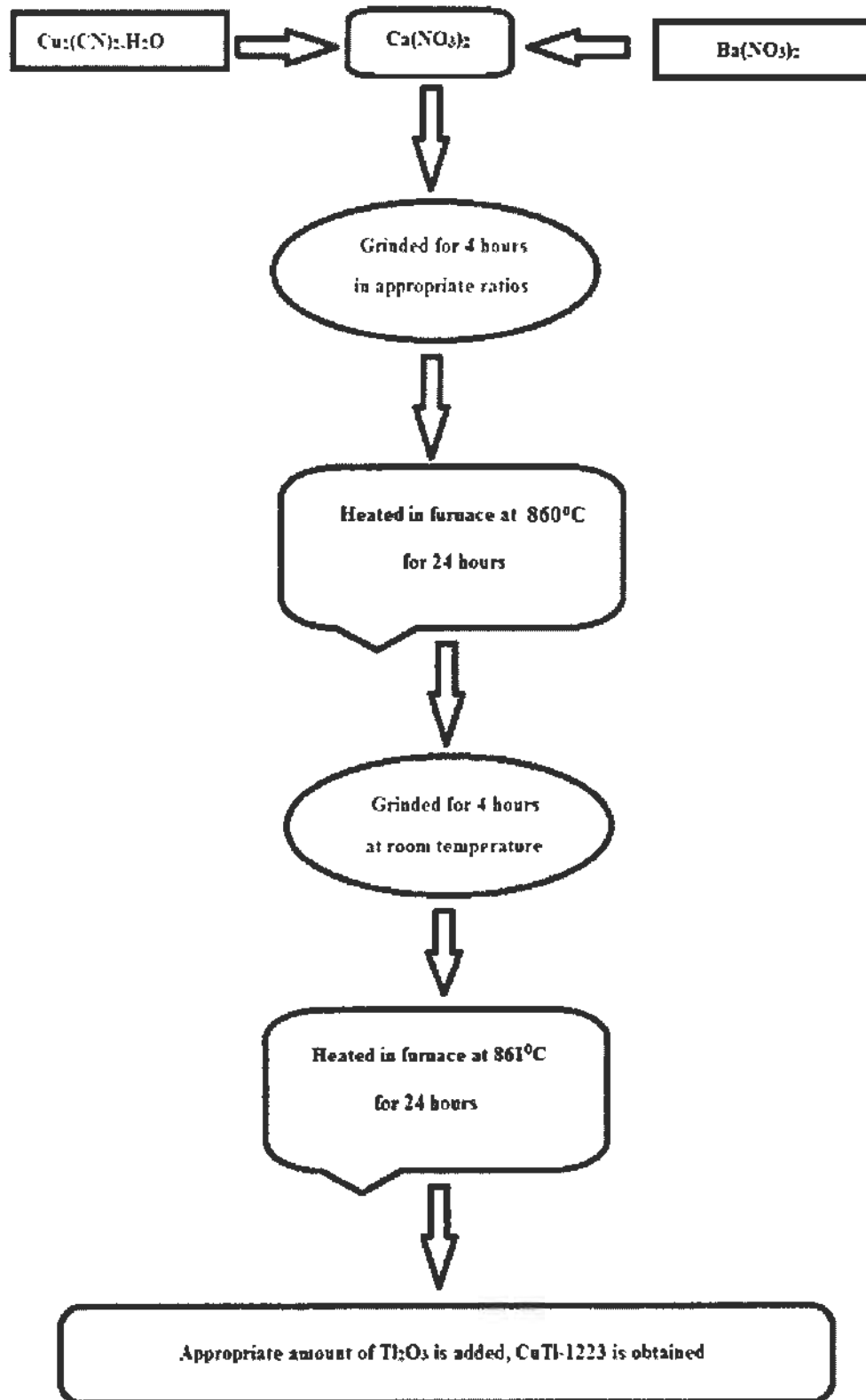
Fig. 3.1: Synthesis process of CuTl-1223.

3.2.3   Synthesis of Al₂O₃/CuTl-1223 superconductor composites

Now I added alumina nanoparticles with different weight i-e x = 0 , 0.5, 1 and 1.5 into CuTl-1223. Then I grounded each composition of precursor and nanoparticle for 1 hour and made pallets at 3.8 tons/cm² with help of hydraulic press. Each pallet was wrapped in gold capsule and placed in furnace at 860°C for 10min. I took care of gold capsule to be air packed so that Tl do not vaporize. All these processes can be explained with help of flow chart given below.
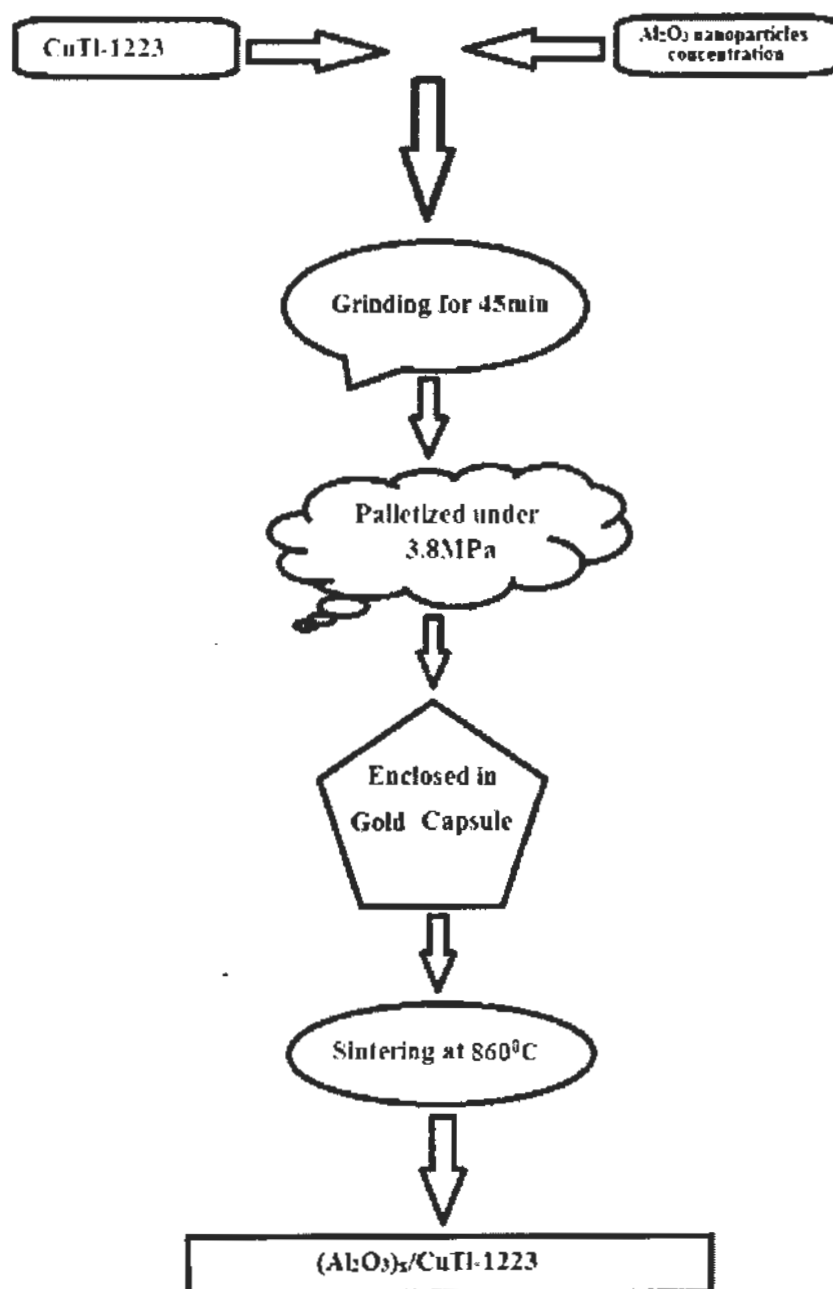
Fig. 3.2: Synthesis of Al₂O₃/CuTl-1223

3.3 Characterization techniques

Techniques which are used to control observations and investigate hypothesis are called experimental techniques. These techniques are used to study structure of atom and its various physical properties. In this way relation between structure and property is observed and advance materials are discovered. There are various materials which are to be investigated like thin films, nanoparticles, metal organic networks, nanotubes protein solutions, superconductors and magnetic materials etc. Experimental techniques which I used are given below.

1. X-ray diffraction (XRD) technique
2. Scanning electron microscopy (SEM)
3. LCR (inductor, capacitor and resistor)
4. Resistivity verses measurement (RT)
5. Energy dispersive X-ray spectroscopy (EDS)

3.4   X-ray diffraction (XRD) technique

XRD is used for investigation of grain size, lattice parameter, phase present and nature of material [3,4].
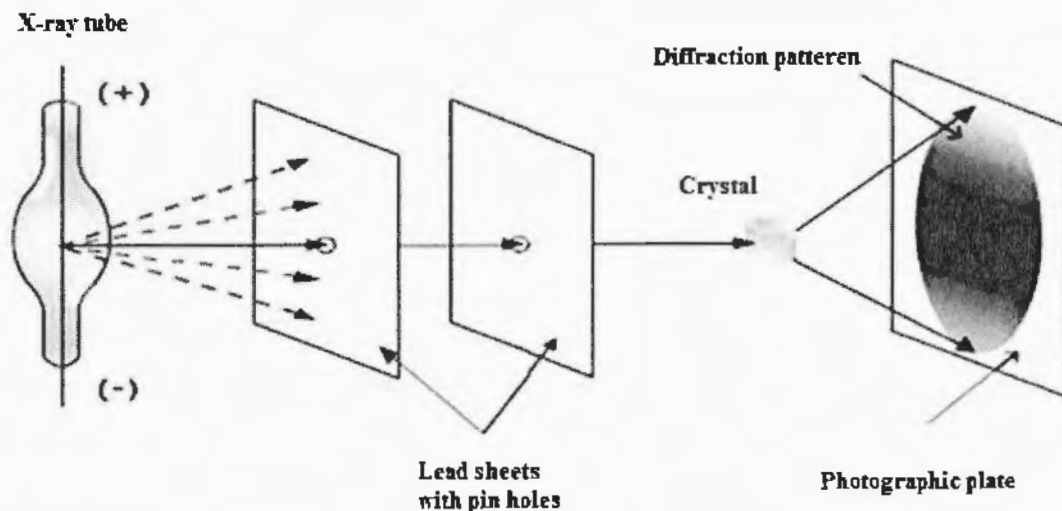
Fig. 3.3: X-ray diffraction technique.

Electromagnetic waves consisting of photons of energy ranging from 100eV to few keV are called X-rays. For diffraction techniques hard X-rays are used. These are rays having short wavelength of only few A^0 to 0.1 A^0. This is necessary because wavelength of X-rays has to be comparable with size of atoms so that conditions for diffraction are satisfied. Hard x-rays

are also capable of penetrating deep into materials so that they can provide internal information of samples. Working diagram of XRD is shown in Fig. 3.3.

3.4.1   Production of X-rays

X-rays are produced whenever a fast moving electron is decelerated due to collision with metal surface and electron loses energy in form of packets of energy, called photons. These high energy photons are called X-rays. Such effect is known as Bremsstrahlung effect. If a fast moving electron knock out an electron from any inner shell of an atom, then electrons from higher shell make transition to fill that shell. In this process the transition electron loses energy in form of x-rays. Such x-rays are known as characteristic X-rays.
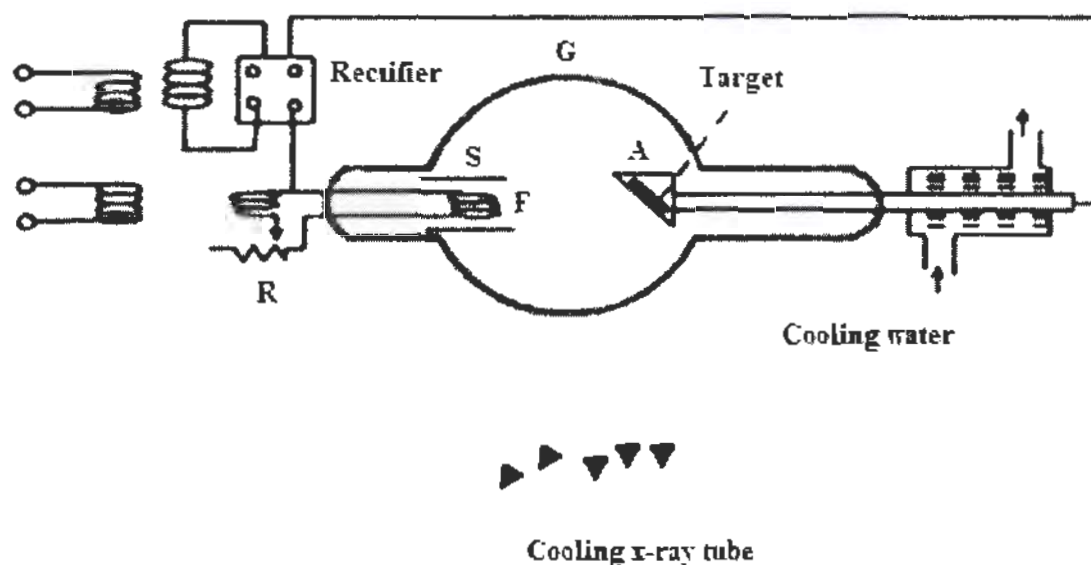
Fig. 3.4: Production of X-rays.

For production of x-rays a vacuum tube is used shown in Fig. 3.4. It contains a heating filament, target and a window. Heating filament emit electrons which are accelerated by applying high voltage. Accelerated electrons hits target and in process x-rays are produced by bremsstrahlung effect or characteristic x-rays. Target is usually made up of tungsten.

3.4.2   Bragg's law

When x-rays are incident on crystal, few x-rays are reflected from first layer and few from second layer as shown in Fig. 3.5. After reflection series of maxima are observed according to following conditions

1. Path difference of two scattered wave should be equal to integral number of wavelengths.

2. Scattering angles are always equal to angle of incidence.
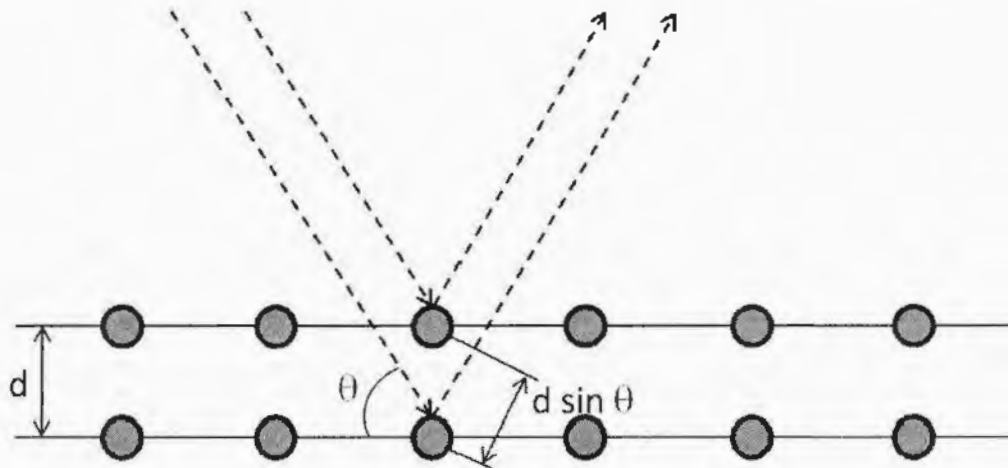
Fig. 3.5: Reflection of X-rays from different layers of crystal.

Using Bragg's law we can calculate wavelength of x-rays if crystal structure is known. Whereas if wavelength is known, then we can determine crystal structure by using following equation.

$$n\lambda = 2d\sin\theta \qquad (3.1)$$

Where λ is wavelength, θ is diffraction angle, d is lattice spacing and n is order of diffraction.

3.4.3 Miller indices

Miller indices are used to find orientation of surface with respect to main crystallographic axes. Fig. 3.6 shows a cubic crystal system, following rules are used purpose for cubic crystal system of a x a x a.
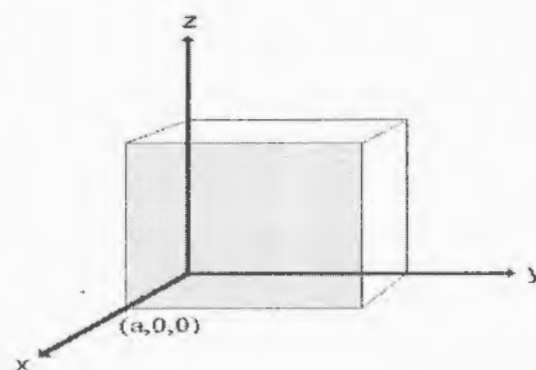
Fig. 3.6: Cubic crystal system.

41

1. Consider following plane, intercept is x = a. Given surface is parallel to z and y axes. So plane will meet at infinity with these axes. Therefore intercepts will be a,∞,∞

2. Take fractional co-ordinates as a/a, ∞/a, ∞/a

3. Give fractional intercepts in reciprocals to form miller indices as (100)

Table.3.1: Crystal structures and their axis angle [5].

No of structures	Crystal structure	Axis	Axis angle
1	Tetragonal	A=B≠C	$\alpha = \beta = \gamma = 90$
2	Monoclinic	A≠B≠C	$\alpha = \gamma = 90, \beta > 90$
3	Triclinic	A≠B≠C	$\alpha \neq \beta \neq \gamma \neq 90$
4a	Rhombohedral	A=B=C	$\alpha = \beta = \gamma \neq 90 < 120$
4b	Hexagonal	A=B≠C	$\alpha = \beta = 90, \gamma = 120$
5	Orthorhombic	A≠B≠C	$\alpha = \beta = \gamma = 90$
6	Cubic	A=B=C	$\alpha = \beta = \gamma = 90$

3.4.4 Lattice spacing in different crystals

Lattice spacing in different crystals can be calculated by using following formulae.

Tetragonal:

$$\frac{1}{d^2} = \frac{h^2 + k^2}{a^2} + \frac{l^2}{c^2}$$

Cubic:

$$\frac{1}{d^2} = \frac{h^2 + k^2 + l^2}{a^2}$$

Hexagonal:

$$\frac{1}{d^2} = \frac{4}{3}\left(\frac{h^2 + hk + k^2}{a^2}\right) + \frac{l^2}{c^2}$$

Orthorhombic

$$\frac{1}{d^2} = \frac{h^2}{a^2} + \frac{k^2}{b^2} + \frac{l^2}{c^2}$$

Monoclinic

$$\frac{1}{d^2} = \frac{1}{\sin^2 \beta}\left(\frac{h^2}{a^2} + \frac{k^2 \sin^2 \beta}{b^2} + \frac{l^2}{c^2} - \frac{2hl \cos \beta}{ac}\right)$$

Rhombohedral

$$\frac{1}{d^2} = \frac{(h^2 + k^2 + l^2)\sin^2 \alpha + 2(hk + kl + hl)(\cos^2 \alpha - \cos \alpha)}{a^2(1 - 3\cos^2 \alpha + 2\cos^3 \alpha)}$$

3.4.5 Different techniques used in XRD

3.4.5.1 Rotating crystal method

In this method a single crystal with its axis normal to monochromatic x-ray is rotated. A diffracted beam is obtained at a point where lattice planes satisfies Bragg angle for incident beam is shown in Fig. 3.7.

(100)

lens

θ_{nc}

transmitter

rotating crystal

θ_{nf}

θ_{so1}

detector
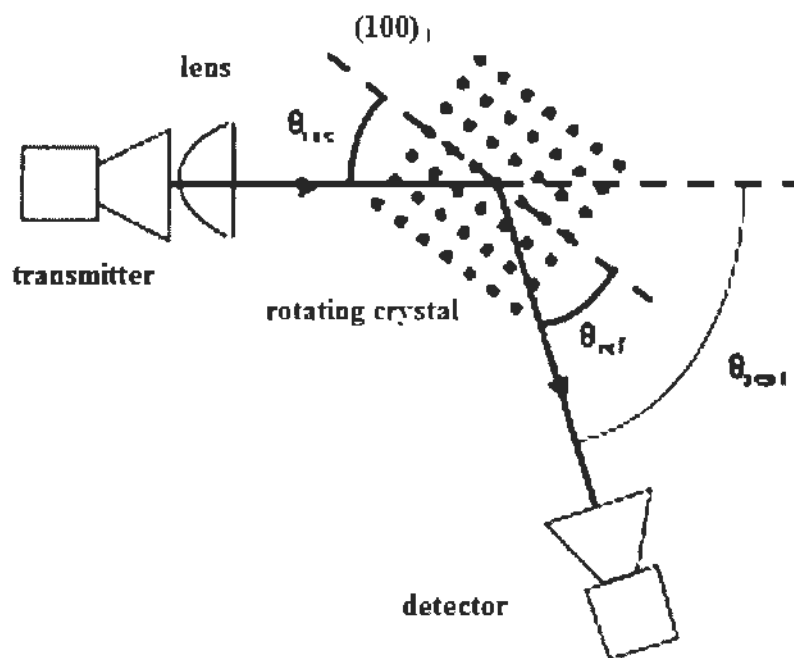
Fig. 3.7: Rotating crystal technique.

There exist imaginary cones where reflected beams are incident. Diffraction spots take horizontal position when film is placed flat. In this way we can observed shape, atomic arrangement and size of unit cell.

3.4.5.2 XRD powder diffraction

Such technique is used to study phase of crystalline materials and investigate dimensions of unit cell. Material used is homogenized, finely grounded and partially bulked composition. Fig. 3.8 shows working diagram of XRD powder diffraction technique.

X-rays are passed through sample and then detected at other end. Samples are scanned at 2θ angles so that all possible diffraction directions are attained. Conversion of peaks into lattice parameters help to identify the mineral. For this purpose lattice spacing is compared with reference patterns.
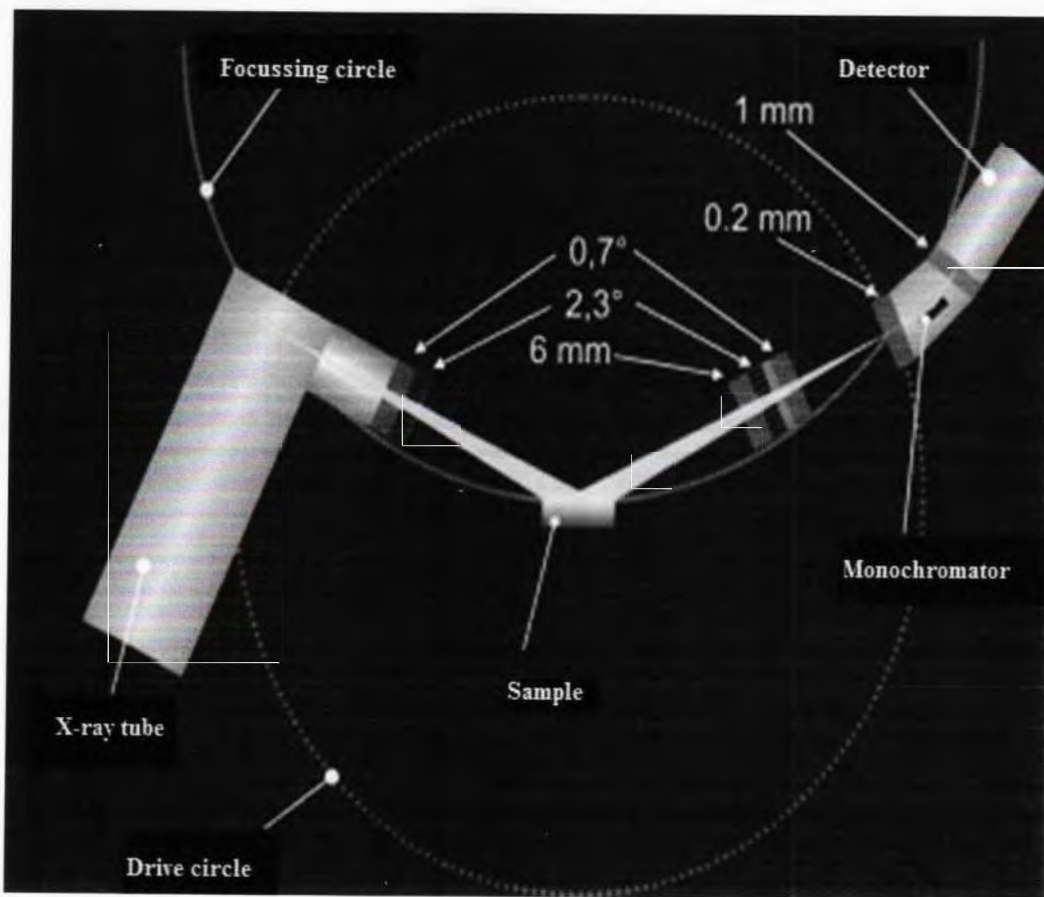
Fig. 3.8: XRD powder diffraction technique.

3.4.5.3 Laue method

Such method is useful for study of orientation of a large single crystals. Fig. 3.9 (a) & (b) shows two variants of Laue method

a). Back-REFLECTION Laue   b). Transmission Laue

Fig. 3.9: Laue Method .

45
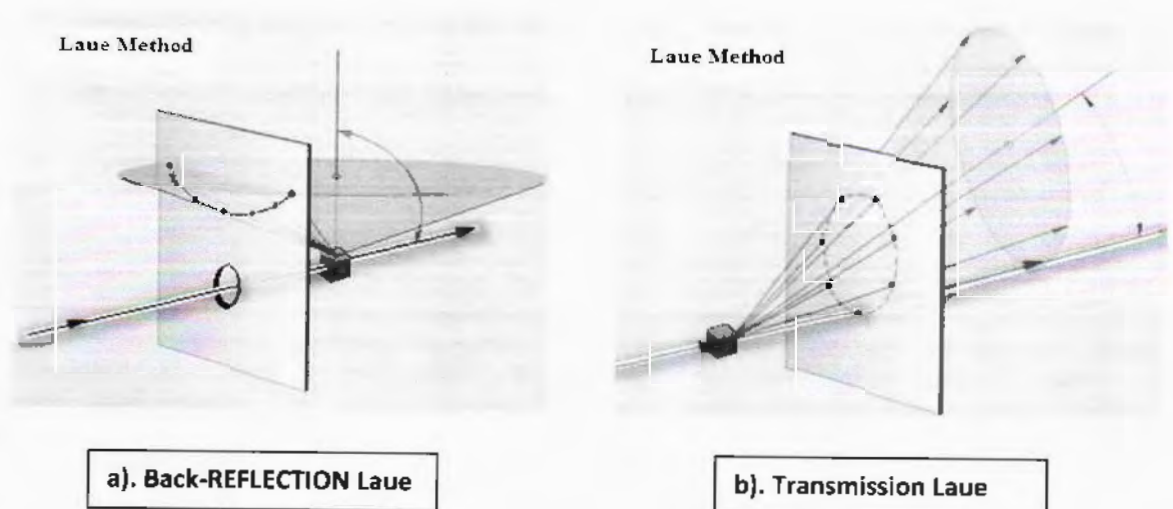
The beam diffracted from crystals form arrays of spots in a pattern of curves on film. For every plane Bragg angle is fixed. Particular wavelength of white light is diffracted from particular plane and satisfies Bragg's law. Each zone reflect a spot on any one curve. There exist zone axis belonging to an imaginary cone that is formed due to Laue reflections from same zone planes.

3.4.5.4 Determinations of particle size

Size of particle can be find by using Debye Scherer formula.
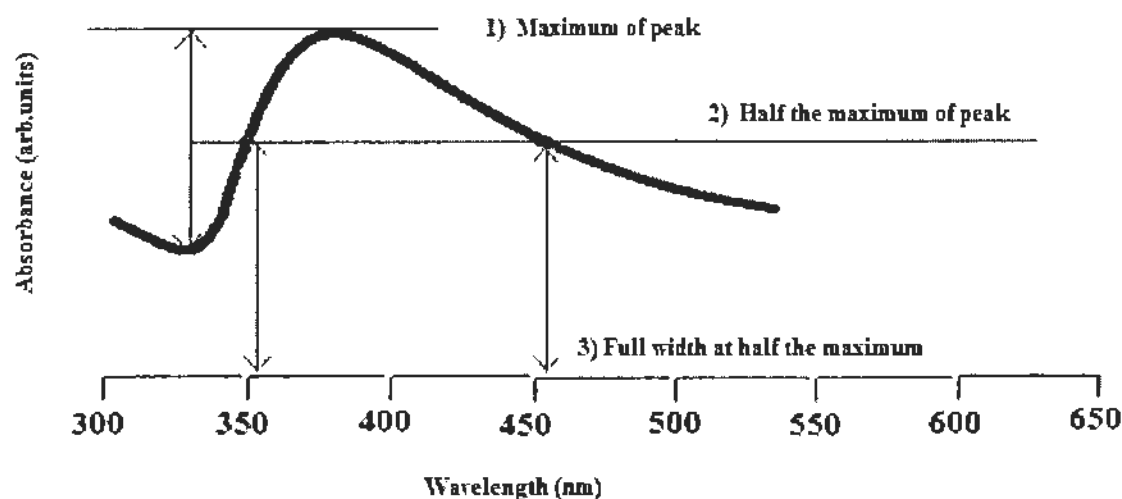
Fig. 3.10: Full width at half maxima .

Debye Scherer formula was proposed by Paul Scherer in 1918. Grain size can be measured up to 0.1 to 0.2 micrometer, more accurately as compared to transmission electron microscope [6]. Formula is given below

$$D = \frac{K\lambda}{\beta\cos\theta} \qquad (3.2)$$

Here K is unit less quantity having value 0.91, D is size of particle to be found, β is FWHM (full width half maximum), λ is wavelength, θ is Bragg's angle having units of radian as shown in Fig. 3.10.

3.5   Energy dispersive X-ray spectroscopy (EDS)

It is a technique which is used for elemental analysis and chemical characterization of sample. Working diagram of EDS is shown in Fig. 3.11. It consists of following components.

1. Source of electron beam
2. Pulse processor

3. Analyser

4. X-ray detector
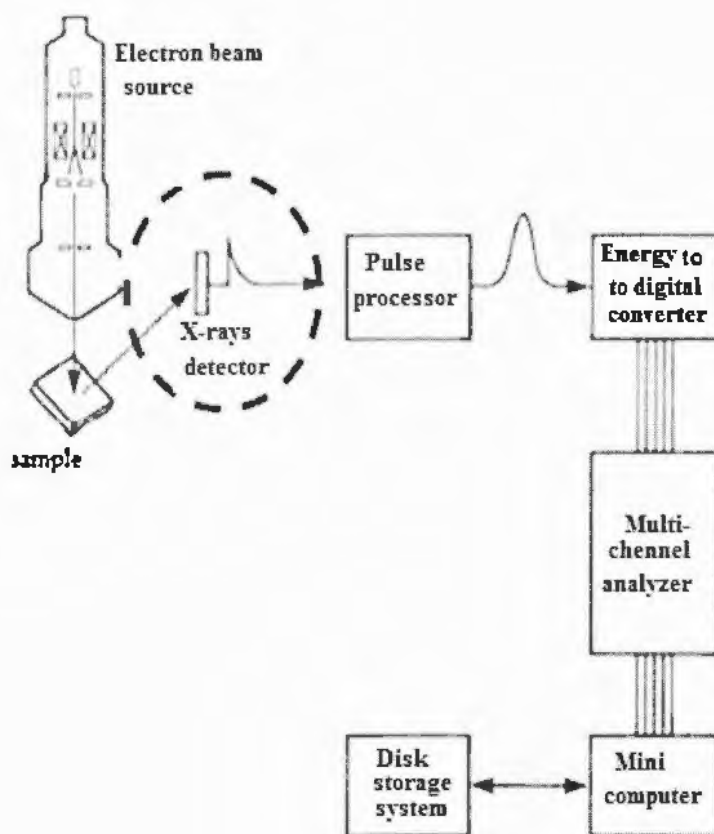
Fig. 3.11 : working diagram of EDS.

An electron beam from source is incident on atoms of sample which results in emission of secondary and backscattered electrons. Secondary electrons emitted from atoms produces holes inside shells. Atoms having holes in inner shells are highly unstable, electrons from outer shell fills the inner shell holes shown in Fig. 3.12. As outer shells possess higher energy level, therefore transition electrons lose their energy. This energy appear in form of x-rays having characteristic energy depending upon parent atoms and shells through which electrons make transition.

For instance in an iron atom if inner most K shell hole is filled by L shell electron, then x-ray photon contains 6400eV energy. If M shell electron fills K shell hole, then x-ray photon contain 7057eV energy. As iron atom has three filled shells, so it may have three peaks. Elements of lower atomic number has less filled shells, so they will have fewer peaks.
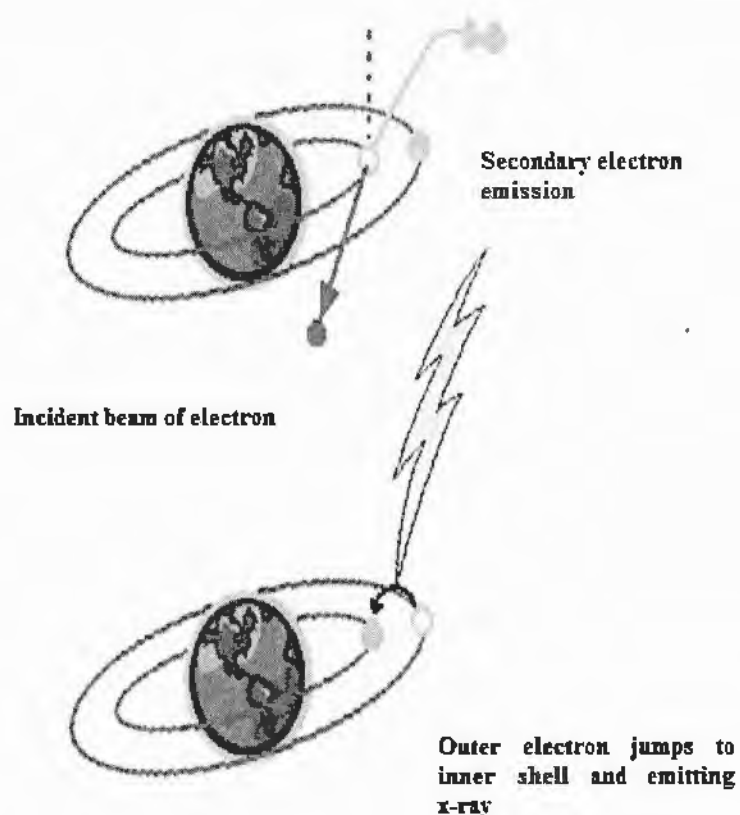
Fig. 3.12: emission of x-ray photon from an atom.

Some high atomic x-rays can have value 50keV but a spectral range of 0-20keV is enough to detect all the elements from boron to uranium. Each element has specific characteristic x-rays spectrum which make it different from other elements.

From EDS we can also find quantity of elements by using standards or standardless analysis. In standardless analysis quantity of elements is calculated by finding area under peak of each element and taking account of accelerating voltage of beam. Then sensitivity factor is used which convert area into atomic percentage. One of software used for it is ZAF, where Z is atomic number, A is absorbance and F is fluorescence. In standard analysis ZAF is not used whereas area calculated is compared with standards files, this analysis is not widely used as it is time consuming.

3.6   LCR meter

LCR is an electronic equipment consisting of inductor, capacitor and resistor shown in Fig. 3.13. It is used to measure capacitance, inductance and resistance of components. By using these three parameters, we can study dielectric properties of sample.

Fig. 3.13: LCR meter.

Measurements are taken out at 100Hz, 120Hz, 1KHz and 10kHz frequencies. Voltage can be provided by a built-in drive ranging from 0.1-1.0V with increments of 50mV. Measurements can be taken at rates of 2, 10 or 20 specimens/sec. For capacitance measurements source of DC is used up to 40V.

3.6.1 Working of LCR meter

1. Sample is placed inside AC voltage source.

2. Digital meter is used to measure current and voltage across sample.

3. Impedance is calculated by ratio of voltage over current.

4. Phase angle between current and voltage and impedance for RL or RC is measured.

5. Digital meter assume a parallel model or series model.

6. RL measurements used elements are placed in series while RC measurements used elements are placed in parallel.

7. Inductance variations are judged with respect to rotor position in machines of permanent magnets.

8. Entire LCR test can be done in quick succession of time, it depends on tested device.

Dielectric constant can be find by using formula,

$$\varepsilon = \epsilon^{/} + i\varepsilon^{//} \qquad (3.3)$$

Real part of dielectric constant can be calculated as,

$$\epsilon^{/} = Cd/\,\epsilon_0\,A \qquad (3.4)$$

Dielectric loss is measured by formula,

$$\tan\delta = 1/2\pi f R_s C_s \qquad (3.5)$$

Imaginary part of dielectric constant can be found as,

$$\varepsilon^{//} = \epsilon^{/}\tan\delta \qquad (3.6)$$

Ac conductivity can be determined by using formula,

$$\sigma_{ac} = \omega\,\epsilon_0\epsilon^{/}\tan\delta \qquad (3.7)$$

3.7   Resistivity measurement

Resistance of a specimen can be measured by applying some current and measuring the voltage response [7]. Resistivity can be measured by using formula

$$\rho = \frac{RA}{L} \qquad (3.8)$$

Where R is resistance, A is area of cross-section, L is length and p is resistivity of specimen.

3.7.1   Resistivity by four probe method

Four probe method is mostly used for measurement of resistivity. It is widely used because it reduces other sources of resistance [8].

Apparatus used in this method include sample, current generator, power supply, digital AVO meter and probe arrangement as shown in Fig. 3.14. Sample is used in form of thin wafer, for this material is deposited on substrate. Sample of size millimetre and thickness w is used. Four probes are used arranged linearly and equally spaced in straight line. In outer two probes a constant current is passed and voltage across inner two probes is measured. To study dependence of sample on temperature, an oven is used that can provide heat to sample.
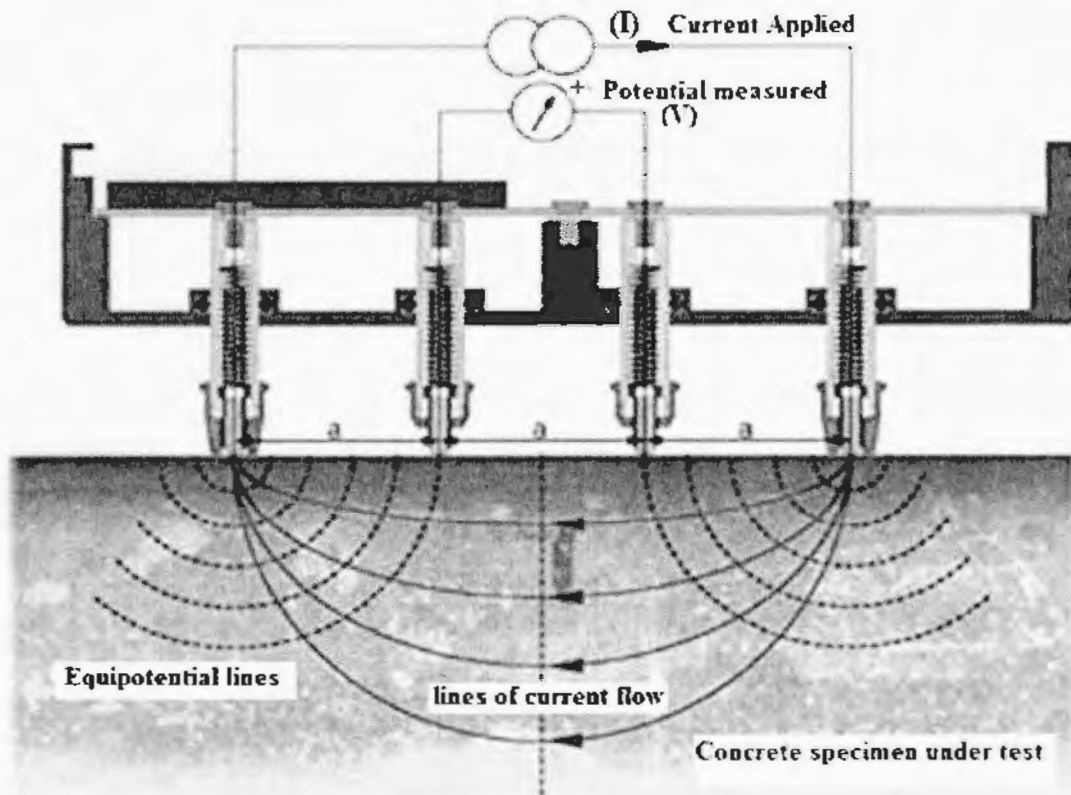
Fig. 3. 14: Four probe method for resistivity measurement.

3.8   Scanning electron microscopy (SEM)

3.8.1   Working principle

Such technique used to generate images of high resolution and chemical composition variations

Several methods are used in SEM which are given below.

1.   EDS (Energy dispersive spectroscopy): used for spot chemical analyses
2.   BSE (Back scattered electron): used for prejudice of phases based on mean atomic no.
3.   CL (Cathode luminescence): used for compositional maps foundation with variations in trace element.

In SEM accelerated electrons of high kinetic energy are used to generate variety of signals by electron sample interactions. Such signals involve secondary electrons, diffracted backscattered electrons, backscattered electrons, photons, visible light and heat as shown in Fig. 3.15.
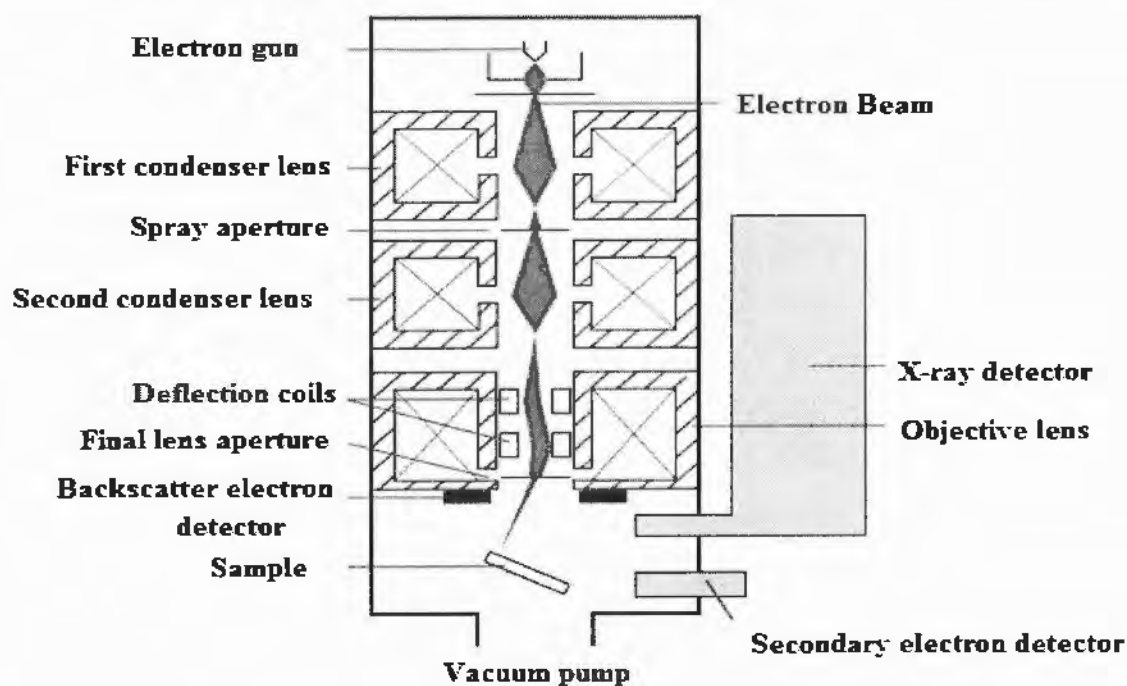
Fig. 3. 15: working diagram of scanning electron microscopy.

Mostly two dimensional images are formed to observe special properties. For this purpose data is collected from particular surface area of material [9].

Morphology and topography is observed by secondary electrons, in multiphase samples contrast in composition is observed by backscattered electrons.

References

1. B. Heeb, S. Oesch, P. Bohac and L. J. Gauckler, "Microstructure of melt-processed $Bi_2Sr_2CaCu_2Oy$ and reaction mechanisms during post heat treatment" J. Mater. Res. **7**, 11 (1992).

2. C. N. Rao and R. Rao, "Chemical insights into High-Temperature Superconductors" Phil. Trans. R. Soc. A **336**, 595 (1991).

3. N. L. Wu, Y. D. Yao, S. N. Lee, S. Y. Wong and E. Ruckenstein, "Synthesis of $Tl_2Ca_nBa_2Cu_n+1O_{6+2n}$ (n=1,2) from Stoichiometric Reactant Mixtures", Physica C **161**, 302 (1989).

4. E. Ruckenstein and S. Narain, "Preparation of XRD single phase 2122 and 2223 compounds by a two-step heating method", Mater. Lett. **8**, 421 (1989).

5. http://ecee.colorado.edu/~bart/book/book/chapter2/ch2_2.htm.

6. D. A. Skoog, D. A. Holler and F.J. Crouch "_ Principles of Instrumental Analysis" sixth Edition, P.456 (2007).

7. J.S. Blakemore, "solid state physics", P.240 (1985).

8. N. Ashcroft and N. Mermin, "Solid state Physics Orlando" Fl Saunders, **346**, 31 (1976).

9. M. Joshi, A. Bhattacharyya and S. W. Ali, "Characterization techniques for nanotechnology applications in textiles" Indian J. Fibre Textile Res. **33**, 304 (2008).

4.1   X-ray diffraction (XRD) analysis

XRD can be commonly used to study the structure of the materials and to measure the average crystallite size. Fig 4.1 shows XRD pattern of alumina (Al_2O_3) nanoparticles. Sherrer's formula is used to find average crystallite size of Al_2O_3 nanoparticles and it is also observed that almost all diffraction peaks are well indexed with cubic structure. It is analysed from XRD pattern that cubic structure and crystallinity with exquisitely indexed planes (3 1 1), (2 2 2), (4 0 0), (5 1 1) and (4 4 0) are in accordance with standard data of international centre for diffraction data (ICDD).
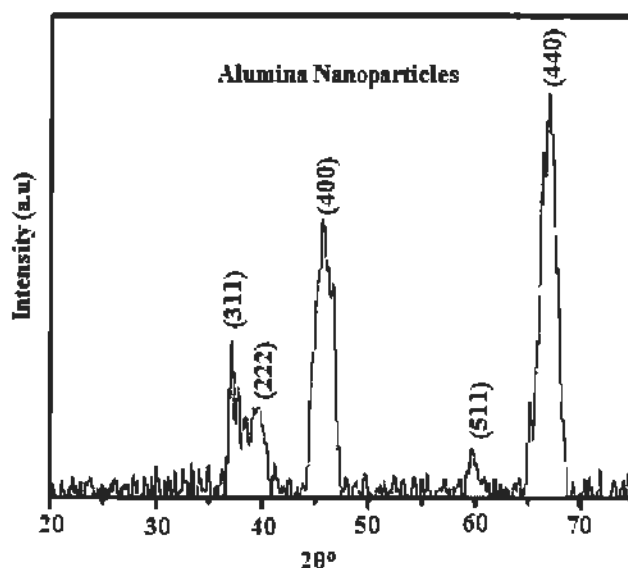
Fig. 4.1: XRD pattern of Alumina nanoparticles.

Fig.4.2(a,b) shows XRD pattern of $(Al_2O_3)_x$/CuTl-1223 (x = 0 and 1.5 wt. %) nanoparticles-superconductor composites. There is no appreciable change in XRD pattern after inclusion of Al_2O_3 nanoparticles, which provides evidence of unaltered stoichiometry and structural chemistry after addition of these nanoparticles. This indicate that nanoparticles have occupied intercrystallite sites of CuTl-1223 matrix which can help to improve weak-links. Other than dominance of CuTl-1223 phase, there are few non-indexed diffraction peaks, which indicates presence of some impurities [1]. The overall stoichiometry of host CuTl-1223 compound remained unchanged after inclusion of these nanoparticles. However, pattern shows slight variations in length of c-axis, which may be due to some strains or oxygen variation.

These variations can result in compression and relaxation of apical bond length of unit cell of CuTl-1223 phase.
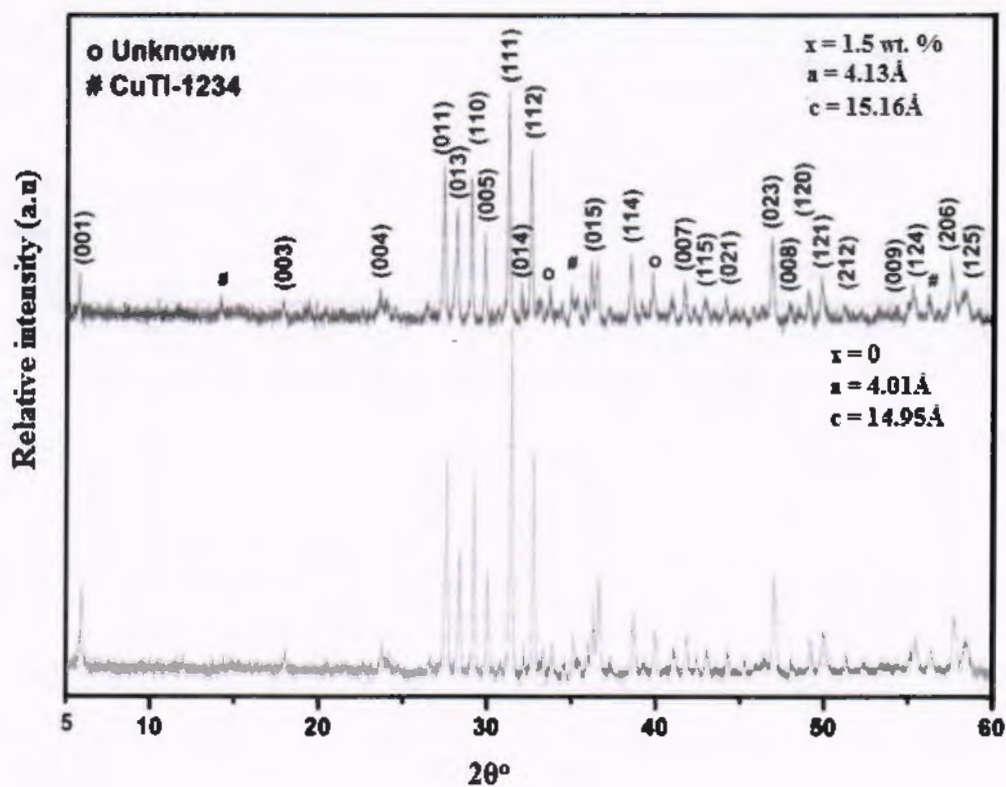
Fig.4.2: XRD patterns for $(Al_2O_3)_x$ /CuTl-1223 (x=0 and 1.5 wt. %) nanoparticles-superconductor composites

4.2 Scanning electron microscopy (SEM) and energy dispersive X-ray (EDX) analysis

SEM is used to investigate morphological properties of $(Al_2O_3)_x$/CuTl-1223 (x=0 and 1.5 wt. %) nano-superconductor composites and is shown in Fig.4.3. It can be seen from SEM images that nanoparticles improved the inter-grain weak links and healed up inter-grain voids in CuTl-1223 matrix. This can be verified from our XRD images that nanoparticles do not penetrated into structure of CuTl-1223 infect they occupied the interstitial spaces. Similar results were reported by different working groups in this field [2].

(a)   (b)

Fig.4.3: SEM images of $(Al_2O_3)_x$/CuTl-1223 (x=0 and 1.5 wt. %) composites.

Fig. 4.4 shows energy dispersive x-ray spectroscopy of $(Al_2O_3)_x$/CuTl-1223 (x=0 and 1.5 wt. %). No peak for Al is found EDX spectrum of $(Al_2O_3)_x$/CuTl-1223 (x = 0), while a reasonable peak of Al is observed in $(Al_2O_3)_x$/CuTl-1223 (x = 1.5 wt. %). Mass percentage of different elements in $(Al_2O_3)_x$/CuTl-1223 composition is given in table 4.1. Similar results were found by other researchers in this field [3, 4].
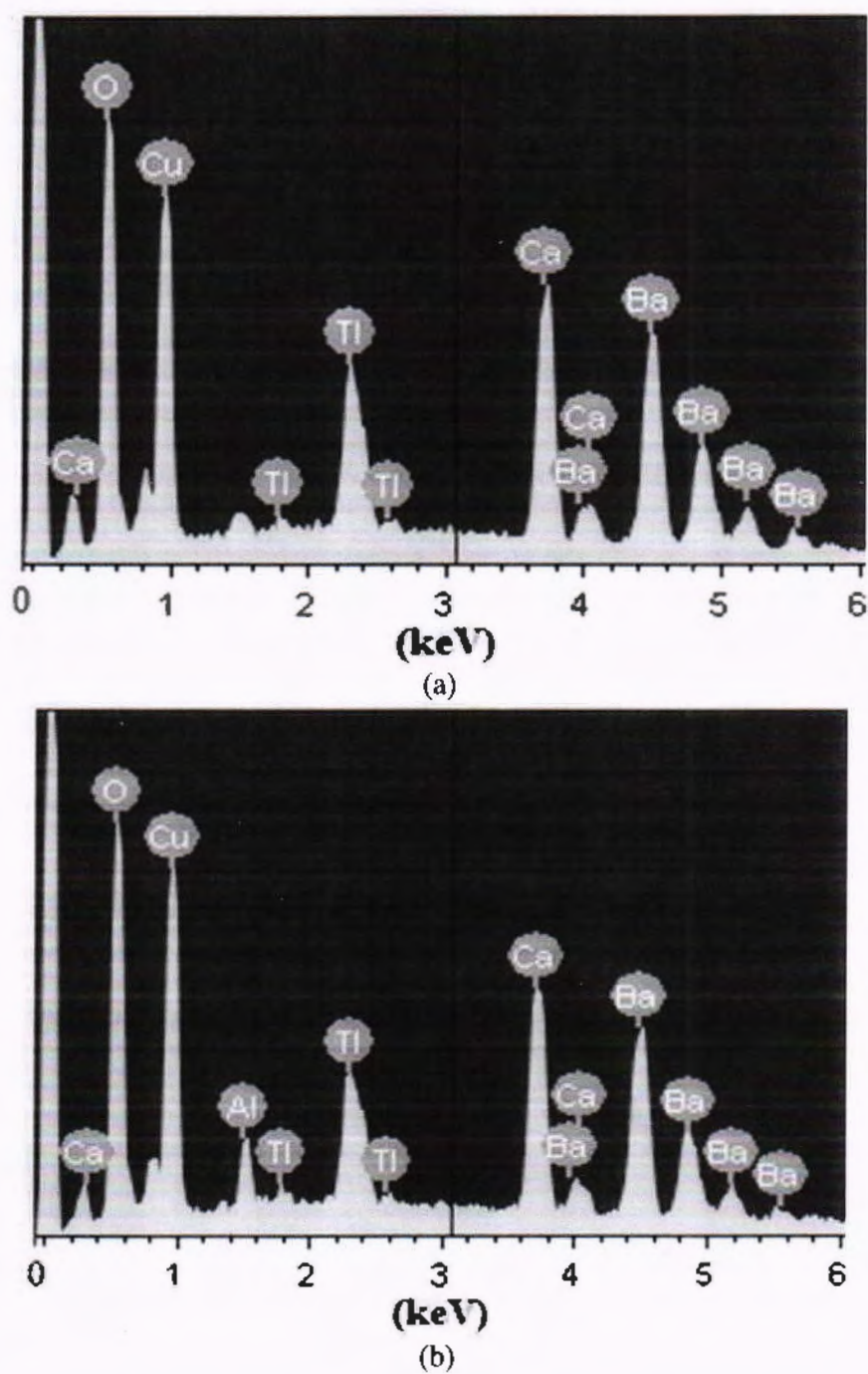
Fig. 4.4: EDX spectra of $(Al_2O_3)_x$/CuTl-1223 (x=0 and 1.5 wt. %) nanoparticle-superconductor composites.

Table 4.1: compositional analysis of $(Al_2O_3)_x$/CuTl-1223 (x=0 and 1.5 wt. %) composite by EDX

Elements S	X = 0			X = 1.5 wt. %		
	keV	Mass %	Atom%	keV	Mass %	Atom%
O K	0.536	20.68	58.05	0.539	18.96	55.31
Ca K	3.693	8.87	9.94	3.696	1.13	1.96
Cu L	0.950	26.93	19.03	0.953	8.69	10.11
Ba L	4.485	31.83	10.41	4.484	24.41	17.92
Tl M	2.324	11.70	2.57	2.327	35.98	12.22
Al K	___	___	___	1.512	10.83	2.47
Total		100	100		100	100

4.3   Resistivity measurements

Measurements of temperature versus resistivity of $(Al_2O_3)_x$/CuTl-1223 (x= 0 and1.5 wt.%) composites are shown in Fig.4.5. Alumina free sample has 'T_c' about 86 K, which is decreased to 65 K after inclusion of nanoparticles; x = 1.5 wt.%, respectively. These values suggest that value of 'T_c' has been suppressed after inclusion of Al_2O_3 nanoparticles in to CuTl-1223 host matrix. The absolute resistivity in normal state may strongly depend on porosity and grain boundary scattering. It is assumed that decrease in 'T_c' is mainly because of insulating behaviour of Al_2O_3 nanoparticles at the grain-boundaries of the host CuTl-1223 superconducting matrix. Reduction of 'T_c' after inclusion of Al_2O_3 nanoparticles may be associated with following reasons;

- Mobile holes trapping
- Fewer oxygen in material
- Oxygen vacancy disorder mechanism [5-9]
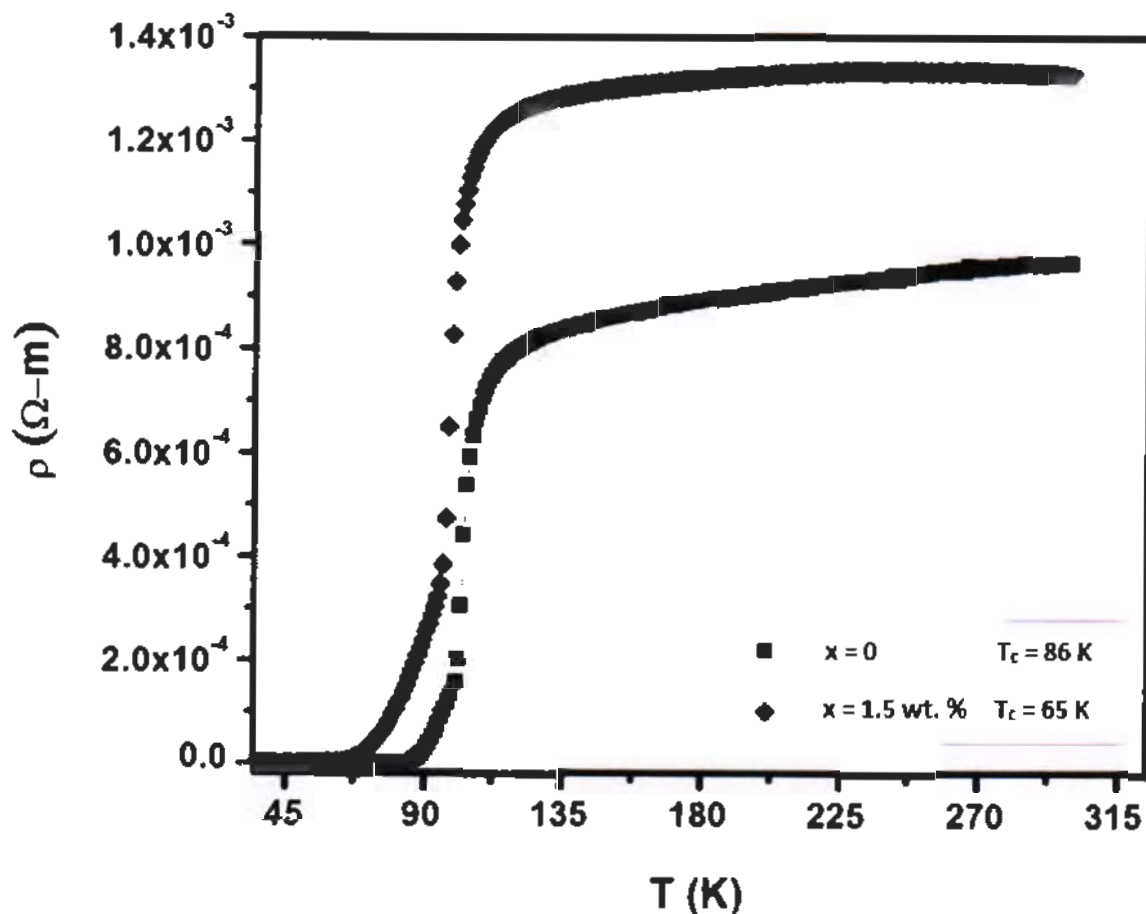
Fig.4.5: Resistivity verses temperature measurements of $(Al_2O_3)_x$ / CuTl-1223 (x = 0 and 1.5 wt. %) nanoparticle-superconductor composites.

4.4   Dielectric measurements

Dielectric properties of $(Al_2O_3)_x$/CuTl-1223 (x = 0, 0.5, 1.0 and 1.5 wt.%) are observed as function of frequency ranges from 10^2 to 10^7 Hz at room temperature. Different parameters of dielectric like capacitance, real part, imaginary part, tangent loss and ac-conductivity have been studied. Dielectric properties of sample are found to be in good agreement with Maxwell-Wagner model, so it is supposed that sample structure has two layers.

- Grain boundaries that behave as poor conductor
- Large grains that behave like good conducting layers

4.4.1 Capacitance

A capacitor is a device which is used to store charge or energy. It consist of two metallic plates which are separated by small distance. The ability of a capacitor to store energy or charge is known as capacitance. Capacitance can be measured for a capacitor by following equation,

$$C = A\varepsilon_0\varepsilon_r/d \qquad (4.1)$$

Where 'C' is capacitance, 'ε_0' is known as permittivity of free space, 'ε_r' is relative permittivity of medium and 'd' is distance between plates. Above equation shows that capacitance depends upon nature of medium, it can be enhanced by placing a suitable material known as dielectric material.

Variations of capacitance of $(Al_2O_3)_x$/CuTl-1223 (x = 0, 0.5, 1 and 1.5 wt. %) samples with frequency ranging from 10^2 to 10^7 Hz are shown in Fig. 4.6. The phenomenon of negative capacitance was observed, which indicate the reduction of sample capacitance as compared to capacitance of electrodes. Phenomenon of dipolar capacitance occurs due to displacement of mobile charge carriers of conducting planes from equilibrium position. Positive space charges may exist at outer surface of device, therefore, free carriers of ceramic sample flows towards metal electrodes. This is because of higher Fermi levels of ceramic superconductor sample as compared to contact electrodes, as ceramics have less filled states than metals and less filled state possess higher energy [10,11].

Sample shows higher value of negative capacitance -3.78 x 10^{-8}, -5.05 x 10^{-9}, 4.60 x 10^{-9}, -1.33 x 10^{-9} F of $(Al_2O_3)_x$/CuTl-1223 (x = 0, 0.5, 1 and 1.5 wt. %) at low frequency 10^2 Hz, which is because of high participation of dielectric polarization. NC decreases with increasing frequency and become minimum at maximum frequency. This is associated with decrease in polarization with increase in frequency.

Peaks are observed in capacitance of $(Al_2O_3)_x$/CuTl-1223 (x = 0, 0.5, 1 and 1.5 wt. %), which may be associated with following of hopping electrons, external field. When the hoping frequency of the electrons is equal to that of the external applied electric field, maximum energy is attained by grains, therefore a peak is obtained in the capacitance and it is called resonance peak. Peaks are shifted towards lower frequency by increasing nanoparticle concentration in CuTl-1223, which may be due to increase in time period of hoping electrons [12].
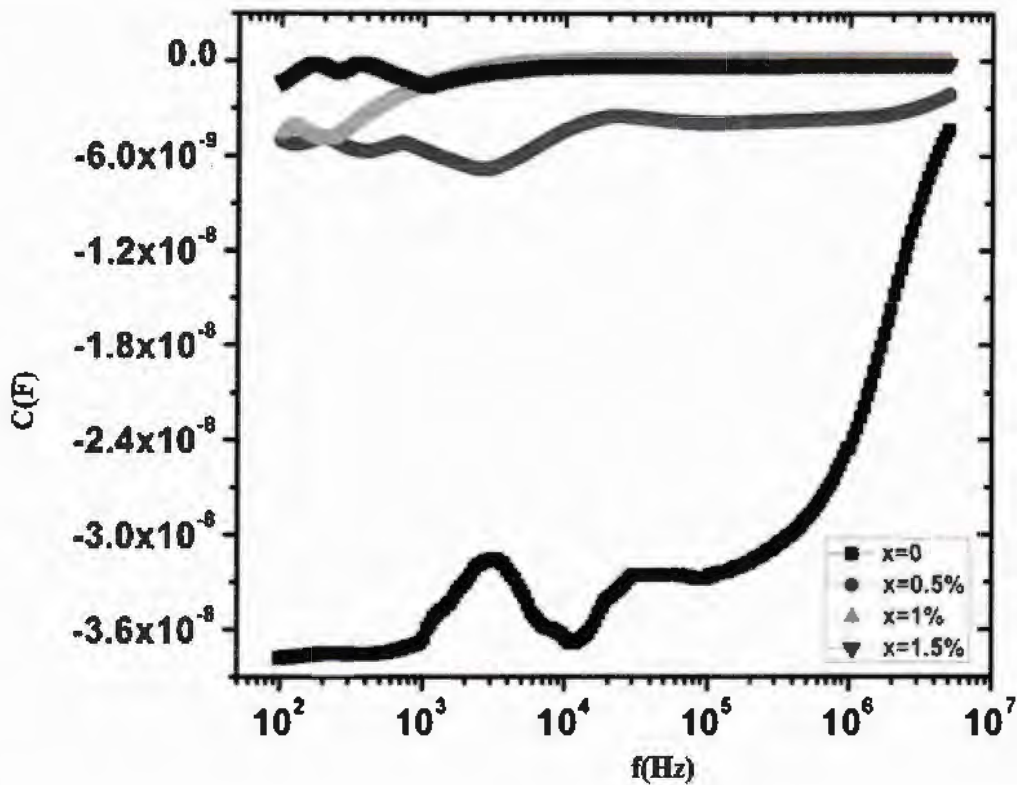
Fig. 4.6: Variation of capacitance of $(Al_2O_3)_x$/CuTl-1223 (x= 0, 0.5, 1.0 and 1.5 wt. %) composites as function of frequency.

4.4.2 Real part of dielectric constant (ε_r')

When electric field is applied on sample, it stores energy. A part of energy is stored within material and rest of energy is lost. The energy stored inside material is represented by 'ε_r'' and energy lost is represent 'ε_r'''. Real part can be found by using following equation

$$\varepsilon_r' = Cd/A\varepsilon_0 \qquad (4.2)$$

Where 'C' is capacitance, 'd' is spacing between metallic plates, 'A' is area of plates and ε_0 is relative permittivity of free space.

Variation of real part of $(Al_2O_3)_x$/CuTl-1223 (x = 0, 0.5, 1.0 and 1.5 wt. %) composites as function of f(Hz) is shown in Fig. 4.7. At low frequency maximum, values of real part were found and it decreases with increasing frequency. This can be explained by using Koop's model and Maxwell-Wagner model [13].

Koop's model consist of two parts, with grain as conducting layers and grain boundaries as non-conducting layers. Electrons enter into grain-boundaries, when field is applied by undergoing hooping process, where electrons piles up and results into polarizations [14]. Real part of dielectric constant decreases at higher frequency because of lagging of electrons to acquire required position i-e grain boundary. When frequency is increased beyond certain

61

point, then there comes a region, where electric field reverses its direction and polarization do not contribute which produces constant values of real part.

Fig. 4.8. shows variation of real part of sample at low frequency of 10^2 Hz, which are -80101.89, -13829.89, -13935.42 and -922.59 for x = 0,0.5,1.0 and 1.5 wt. %. Value of real part decreases that may be due to increase in main phase volume fraction, improvement in microstructure, reduction of electrical inhomogeneity and healing of microcracks which increases connectivity between grains.
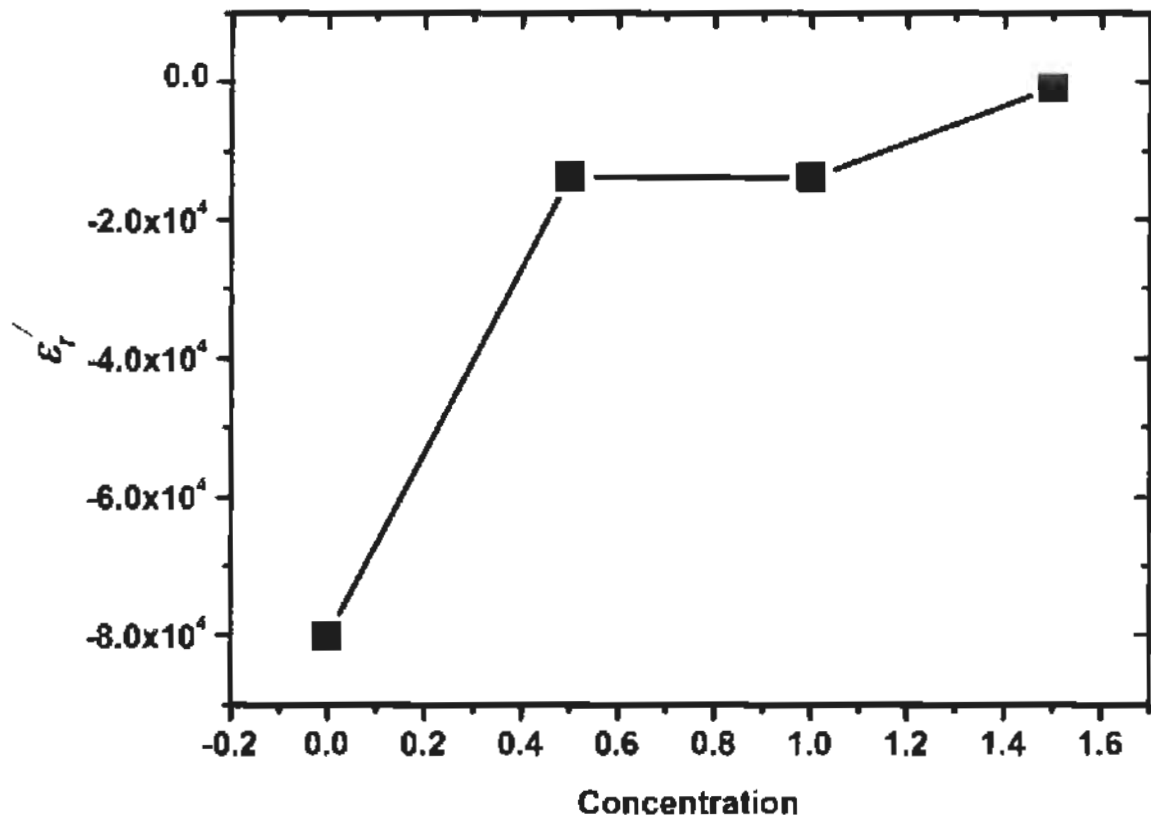
Fig. 4.7: Variation of real part of $(Al_2O_3)_x$/CuTl-1223 (x= 0, 0.5, 1.0 and 1.5 wt. %) composites at 100Hz frequency.

Peaks are observed in real part of $(Al_2O_3)_x$/CuTl-1223 (x= 0, 0.5, 1 and 1.5 wt. %), which may be associated with dielectric resonance. When the frequency of hoping electrons and external applied electric field become equal, then real part become maximum. Peaks are shifted towards lower frequency by increasing nanoparticle concentration in CuTl-1223, which may be due to increase in time period of hoping electrons [15].
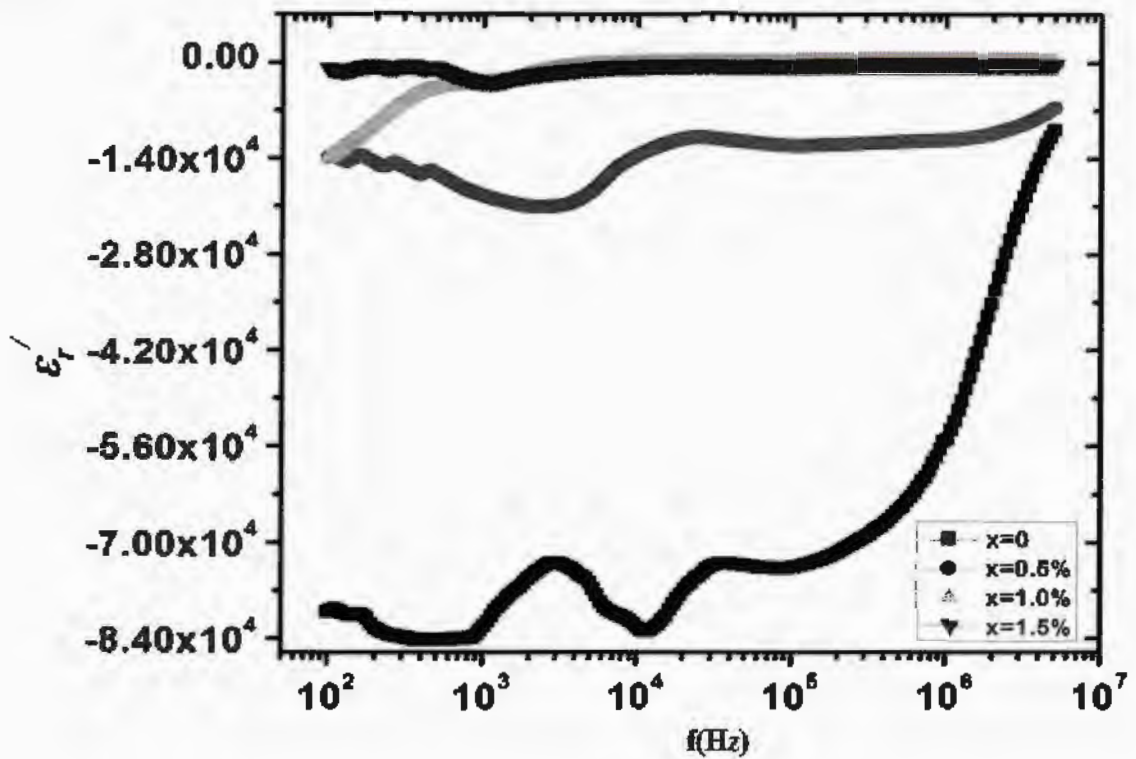
Fig. 4.8: Variation of real part of $(Al_2O_3)_x$/CuTl-1223 (x= 0, 0.5, 1.0 and 1.5 wt. %) composites as function of frequency.

4.4.3 Imaginary part (ε_r'')

The attenuation and absorption of energy across interface when material is exposed to electric field can be described by imaginary part (ε_r'') of dielectric constant, which can be calculated by using following formula;

$$\varepsilon_r'' = \varepsilon_r' \tan\delta \qquad (4.3)$$

Energy absorption exist across interface because of grain-boundaries, defects, dislocations and disorientations. 'ε_r''' is maximum at low frequency of 10^2Hz which is calculated as, -1.11×10^9, -6.48×10^8, -3.35×10^7 and -9.81×10^7 for concentrations of nanoparticles as x = 0, 0.5, 1 and 1.5 wt.%, respectively. Attenuation of energy at low frequency of 10^2 Hz is shown in Fig. 4.9.

Fig. 4.9: Variation of imaginary part of $(Al_2O_3)_x$/CuTl-1223 (x= 0, 0.5, 1.0 and 1.5 wt. %) composites at 100Hz frequency.

Decrease in negative values of attenuation of energy is observed with increasing concentration x = 0 to 1.0 wt.% then increases for 1.5 wt. %. Variation in 'ε_r''' of $(Al_2O_3)_x$/CuTl-1223 (x = 0, 0.5, 1.0 and 1.5 wt. %) composites as function of f(Hz) at room temperature is shown in Fig. 4.10. Behaviour of dielectric dispersion is according to Maxwell-Wagner model and Koop's theory. Dispersion decreases rapidly in lower frequency region and it becomes frequency independent after 10^4 Hz.

Here sample is assumed to be consisted of conducting grains with poorly conducting grain boundaries [16]. It can be seen that electrical conducting grains are less effective than grain boundaries at lower frequencies. At higher frequencies 'ε_r''' decreases that may be due to decrease in polarization, while at lower frequency' ε_r'''increases due to high effect of polarization.
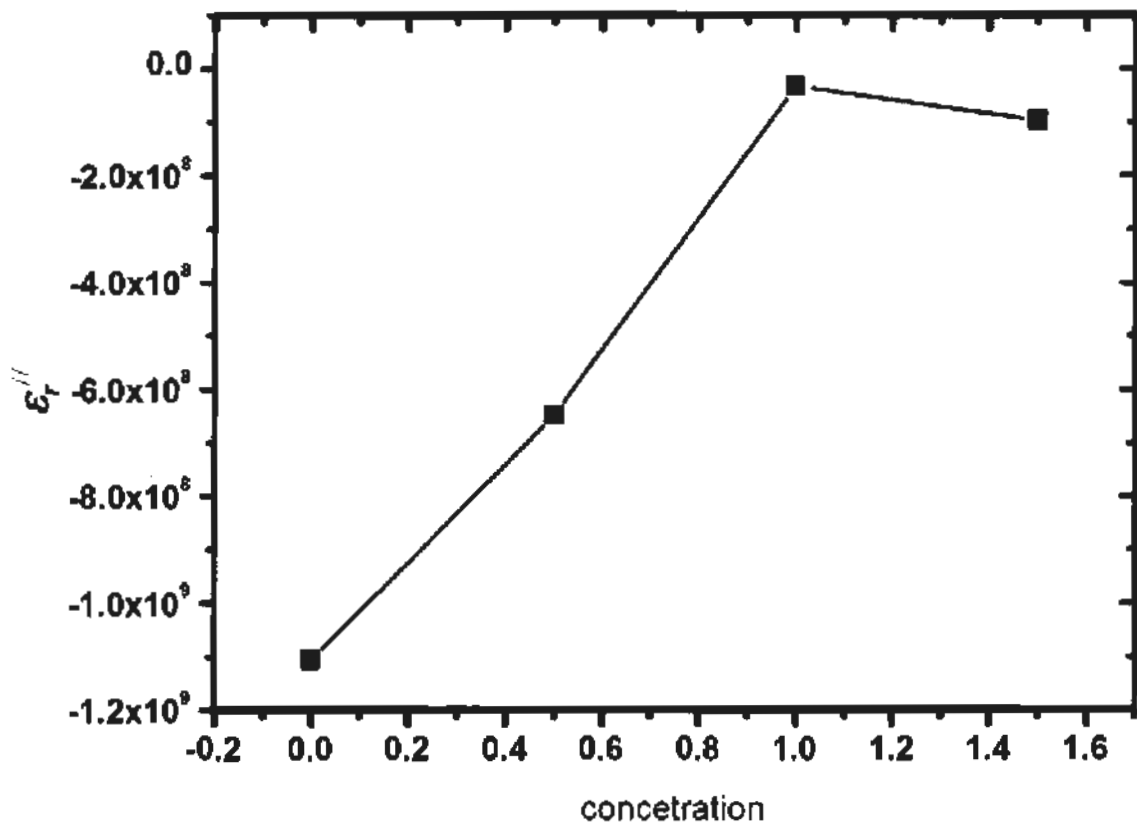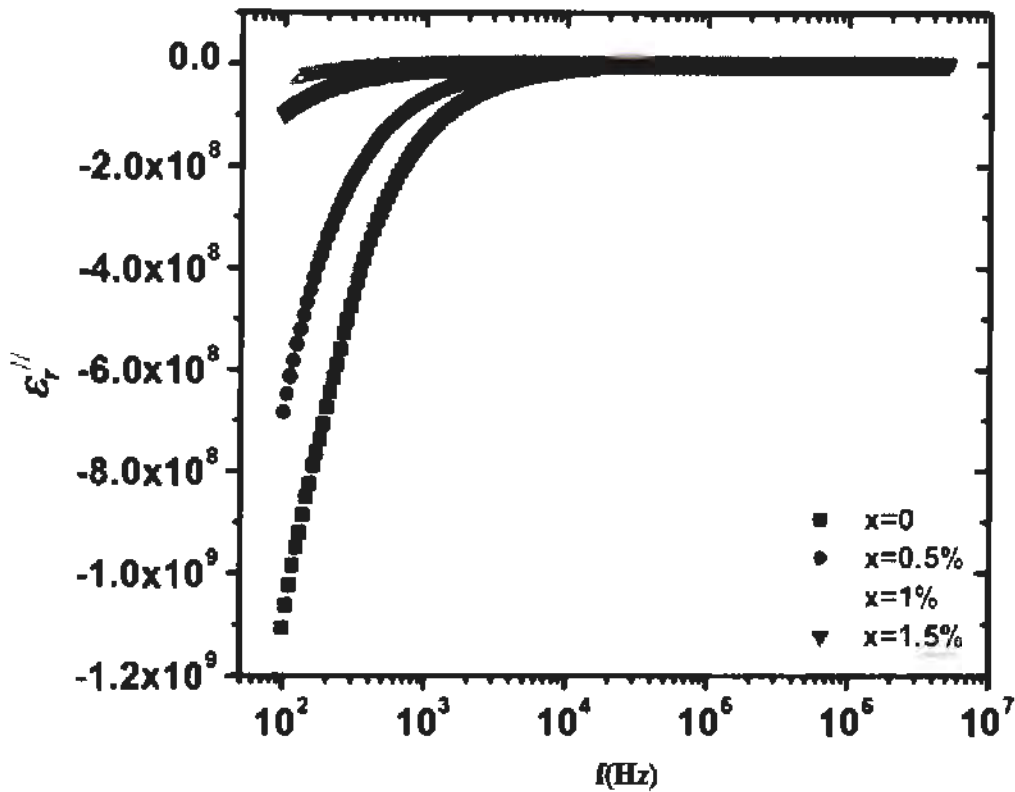
Fig. 4.10: Variation of imaginary part of $(Al_2O_3)_x$/CuTl-1223 (x= 0, 0.5, 1.0 and 1.5 wt. %) composites as function of frequency.

4.4.4   Dielectric loss tangent (tanδ)

Amount of energy loss inside the material can be estimated by tangent loss 'tanδ'. It is defined as the ratio of energy lost in grain boundaries to energy stored inside grains and is given by equation,

$$tan\delta \ = \ \frac{\varepsilon_r^{''}}{\varepsilon_r^{'}} \qquad (4.4)$$

The phenomenon of dielectric relaxation and ac-conduction can be explained on basis of dielectric loss factor. Supreme value of 'tanδ'of $(Al_2O_3)_x$/CuTl-1223 at lowest possible frequency 10^2 Hz are calculated around 1.9×10^4, 4.3×10^4, 0.2×10^4 and 2.09×10^4 for concentrations of nanoparticles as x = 0, 0.5, 1.0, and 1.5 wt. %, respectively. At low frequency 'tanδ' has minor values, which may be associated with dominant behaviour of grain-boundaries, where hopping charges piles up and resulting in high values of real part of dielectric constant.

Peaks are observed in 'tanδ' after inclusion of nanoparticles at different frequencies, which are 5.5×10^5 at 175 Hz, 4.8×10^5 at 130 Hz, 0.2×10^5 at 210 Hz and 7.1×10^5 at 245 Hz for concentrations x=0 , 0.5, 1.0 and 1.5 wt. %, respectively. These peaks indicate relaxation

process, peak is observed when period of applied field is closer to electrical dipoles relaxation time. Variation of values of 'tanδ' of $(Al_2O_3)_x$/CuTl-1223 and f(Hz) is shown in Fig. 4.11 and variations in peaks of 'tanδ' with frequency are shown in inset. Peak positions shifts towards higher frequency after addition of nanoparticles and maximum peak is observed at x = 1.5 wt. %. Shifting of peaks towards higher frequency may be due to decrease in relaxation time with increasing concentration. Broadening of tangent loss peaks suggests different relaxation time which may be associated with additional spatial charge polarizations in grain boundaries and interfaces because of inhomogeneous electrical behaviour. It can be minimized by improving microstructures of samples [17].
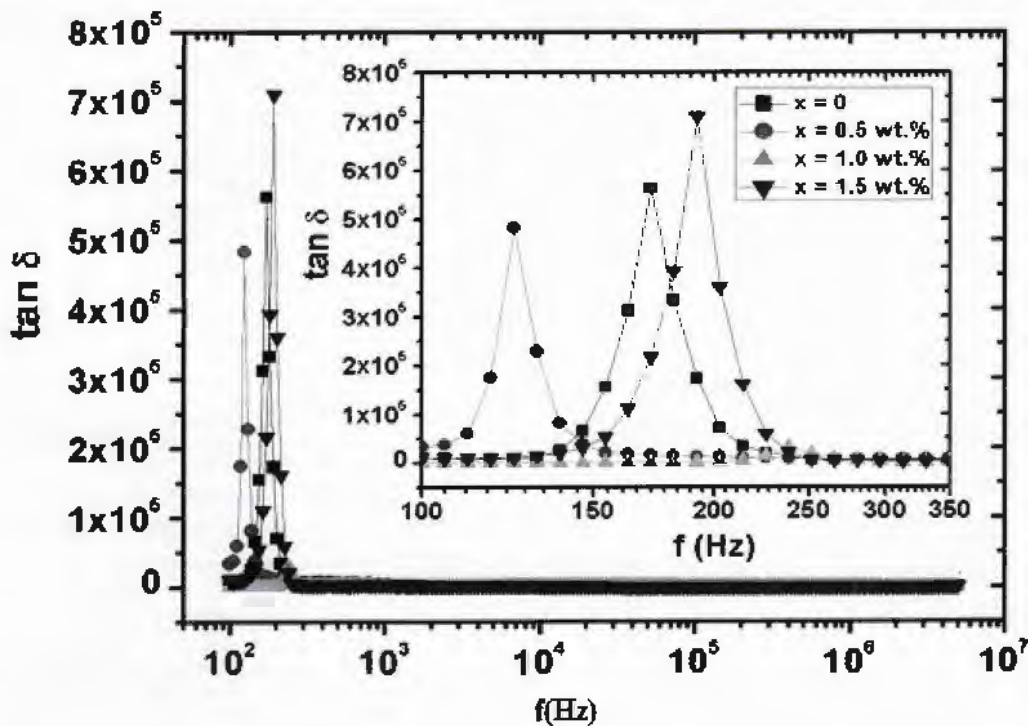

Fig. 4.11: Variation of tangent loss of $(Al_2O_3)_x$/CuTl-1223 (x= 0, 0.5, 1.0 and 1.5 wt. %) composites as function of frequency.

4.4.5 Ac Conductivity

Ac conductivity of sample is determined by using following equation

$$\sigma_{ac} = \omega\ \varepsilon_r'\ \varepsilon_0\ \tan\delta \qquad (4.5)$$

It depends upon angular frequency $\omega = 2\pi f$, tangent loss tanδ, permittivity of free space 'ε_0' and real part of dielectric constant 'ε_r''.

The variation in values of ac-conductivity of $(Al_2O_3)_x$/CuTl-1223 (x = 0,0.5,1.0 and 1.5 wt.%) as function of frequency ranging from 10^2 to 10^7 Hz is shown in Fig 4.12. The maximum negative value of ac-conductivity was found at frequency 10^2 Hz, which is -7.875,-3.807,-0.186

and -0.545 x = 0, 0.5, 1.0 and 1.5 wt. %. Decrease in 'σ_{ac}'is observed after inclusion of nanoparticles in sample, which may be because of insulating nature of Al_2O_3 nanoparticles and charge carriers density is decreased at grain-boundaries.

Ac-conductivity has lower value at high frequency of 5×10^6 Hz, which increases with decreasing frequency. But it become almost independent of frequency beyond 10^5 Hz, which may be due to the reason that time constant of applied signal become shorter than time constant of dipolar polarization [18].
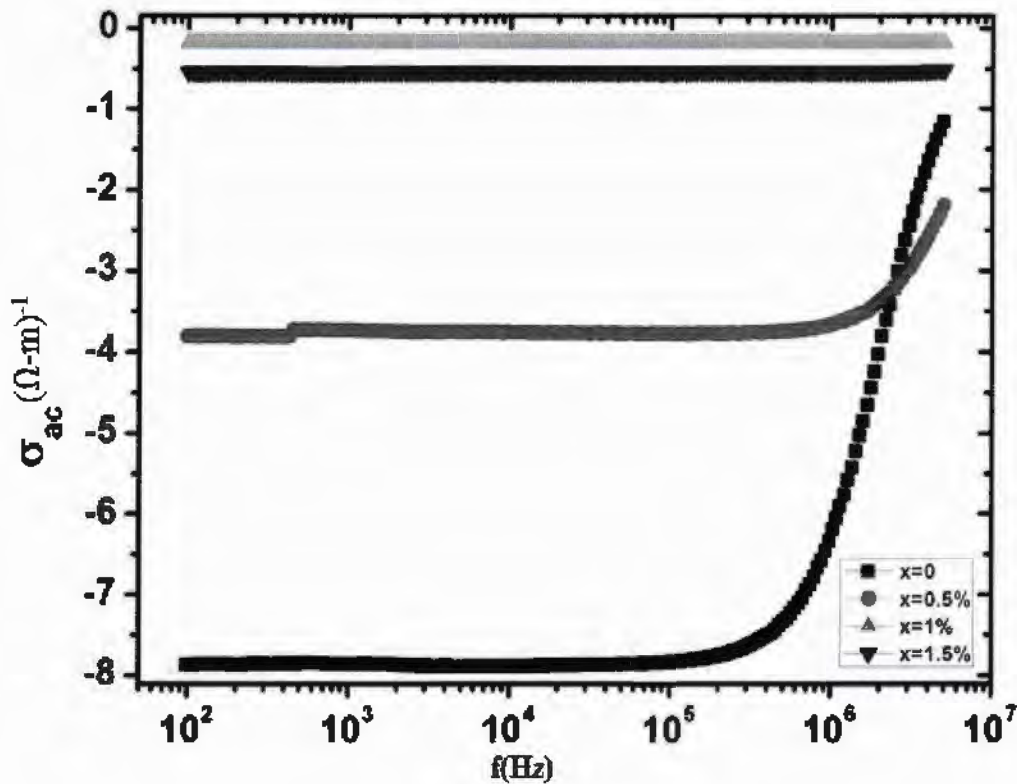

Fig. 4.12: Variation of ac-conductivity w of $(Al_2O_3)_x$/CuTl-1223 (x= 0, 0.5, 1.0 and 1.5 wt. %) composites as function of frequency.

Conclusion

Series of $(Al_2O_3)_x$/CuTl-1223 (x = 0, 0.5, 1.0 and 1.5 wt. %) nanoparticle-superconductor composites were synthesized successfully by sol-gel/solid state reaction method and characterized by different experimental techniques. Structural, morphological, composition, superconducting and dielectric properties were explored by XRD, SEM, EDX, RT and LCR, respectively. Granular structure with enhanced grain sizes can be seen by SEM micrographs. Tetragonal crystal structure of CuTl-1223 matrix was not altered after the addition of Al_2O_3 nanoparticles, which provides a clue about their occupancy at the grain-boundaries in the bulk CuTl-1223 material. Presence of Al_2O_3 nanoparticles in bulk CuTl-1223 sample was confirmed by EDX spectra. The suppression of superconducting properties can be attributed due to the insulating nature of Al_2O_3 nanoparticles, which can minimize the mobility of the carriers. Dielectric parameters have been decreased with the increase of frequency and became saturated at higher frequencies. The ac-conductivity (σ_{ac}) of $(Al_2O_3)_x$/CuTl-1223 (x= 0, 0.5, 1.0 and 1.5 wt. %) nano-superconductor composites was decreased with increasing wt. % of Al_2O_3 nanoparticles, which is associated with insulating nature of Al_2O_3.

References

1   A. Jabbar, I. Qasim, M. Waqee-ur-Rehamn, M. Zaman, K. Nadeem and M. Mumtaz, "Structural and superconducting properties of $(Al_2O_3)_y$/CuTl-1223 composites" J. Electron. Mater. **44**, 110 (2015).

2   A. Mellekh, M. Zouaoui, F. B. Azzouz, M. Annabi and M. Ben Salem, "Nano- Al2O3 particle addition effects on $YaBa_2Cu_3O_y$ superconducting properties" Solid Stat. Commun. **140**, 318 (2006).

3   N. H. Mohammad, A. I. Abou-Aly, I. H. Ibrahim, R. Awad and M. Rek-aby, "Effect of Nano-Oxides Addition on the Mechanical Properties of $(Cu_{0.5}Tl_{0.5})$-1223 Phase" J. Alloys Comp. **486**, 733 (2009).

4   A. Mellekh, M. Zouaoui, F. B. Azzouz and M. B. Salem, "Nano- Al_2O_3 particle addition effects on Y $Ba_2Cu_3O_y$ superconducting properties" Solid State Commun. **140**, 318 (2006).

5   X. F. Rui, J. Chen, X. Chen, W. Guo, and H. Zhang, " Superconductivity and its Applications" Physica C **412**, 312 (2004).

6   M. Zouaoui, A. Ghattas, M. Annabi, F. B. Azzouz and M. B. Salem, "Magneto-resistance analysis of nanometer Al_2O_3 added Bi-2223 polycrystalline superconductors" J. Phys. Conference Ser. **150**, 309 (2009).

7   M. Annabi, A. Ghattas, M. Zouaoui, F. B. Azzouz and M. B. Salem, "Fluctuation conductivity in nano-sized Al_2O_3 added (Bi,Pb)-2223 superconductors under applied magnetic field" J. Phys. Conference Ser. **150**, 520 (2009).

8   M. Mumtaz, and N. A. Khan, "Dielectric response of $Cu_{0.5}Tl_{0.5}Ba_2(Ca_{2-y}Mg_y)$ $(Cu_{0.5}Zn_{2.5})O_{10-\delta}$ bulk superconductor to frequency and temperature" Physica C **469**, 182 (2009).

9   M. Mumtaz, and N. A. Khan," Dielectric response of $Cu_{0.5}Tl_{0.5}Ba_2(Ca_{2-y}Mg_y)$ $(Cu_{0.5}Zn_{2.5})O_{10-\delta}$ bulk superconductor to frequency and temperature" Physica C **469**, 728 (2009).

10 N. A. Khan, M. Mumtaz and A. A. Khurram, "Frequency dependent dielectric properties of $Cu_{0.5}Tl_{0.5}Ba_2Ca_2Cu_{3-y}Zn_yO_{10+\delta}$ (y= 0, 1.0, 1.5, 2.0, 2.5) superconductors" J. Appl. Phys. **104**, 339 (2008).

11 J. C. M. Peko, "Effect of negative capacitances on high-temperature dielectric measurements at relatively low frequency" Appl. Phys. Lett. **71**, 3730 (1997).

12 P. Kuruva, P. R. Matli, B. Mohammad, S. Reddigari and S. Katlakunta "Effect of Ni–Zr codoping on dielectric and magnetic properties of $SrFe_{12}O_{19}$ via sol–gel route" J. of Magn. and Mag. Mater. **382**, 172 (2015).

13 K.W. Wagner, "Dielectric properties of polycrystalline mixed nickel–zinc ferrites" Anal. Phys., **40**, 817, (1913).

14 D. J. Griffiths, "Introduction to Electrodynamics", 3rd ed, Prentice Hall, Upper Saddle River, NJ, P. 161.

15 C. C. Wang, H. B. Lu, K. J. Jin and G. Z. Yang, "Temperature-Dependent Dielectric Strength of a Maxwell-Wagner Type Relaxation" Appl. Phys. Lett. **22**, 1297, (2008).

16 N. H. Mohammed, "Effect of MgO Nano-oxide Additions on the Superconductivity and Dielectric Properties of $Cu_{0.25}Tl_{0.75}Ba_2Ca_3Cu_4O_{12-\delta}$ Superconducting Phase" J. supercond., **11**, 1207 (2011).

17 X. Jiao, Z. Fu, M. Feng, L. Xu, K. Zuo and R. Chen,, "Dielectric studies in a layered Ba based Bi-2222 cuprate $Bi_2Ba_2Nd_{1.6}Ce_{0.4}Cu_2O_{10+\delta}$" Physica C **417**, 166 (2009).

18 A. Younis* and N. A. Khan, "Dielectric Properties of $Cu_{0.5}Tl_{0.5}Ba_2Ca_3Cu_{4-y}Zn_yO_{12-\delta}$ (y = 0, 3) Superconductors" J. Korean Phys. Soc. **47**, 1437 (2010).